NTNU

Norwegian University of
Science and Technology

Automatic Detection for MTI Processed Radar Signals

Morten Ihlen

Master of Science in Electronics
Submission date: June 2011
Supervisor: Morten Olavsbråten, IET
Co-supervisor: Yngve Steinheim, SINTEF IKT

Norwegian University of Science and Technology
Department of Electronics and Telecommunications

Oppgavebeskrivelse

SINTEF og Radian AS på Kongsberg arbeider for tiden med nye metoder for bedring av deteksjonsevne for navigasjonsradar. En av metodene går ut på å forbedre deteksjon av bevegelige mål ved å ta i bruk adaptive digitale dopplerfiltre. Dette kalles også MTI (Moving Target Indicator) eller puls-doppler prosessering. Slike filtre demper ekko fra uinteressante objekter (sjø, regn) ved å estimere deres midlere dopplerfrekvens og dernest legge et båndstoppfilter på denne frekvensen. Arbeidet så langt viser at MTI signalbehandling på disse forholdsvis enkle og billige radarsystemene er mulig. Forsøkene med behandling av reelle radarsignaler er godt i gang og en arbeider nå med å få frem en teknologidemonstrator som kan vise et MTI-behandlet radarbilde i nær sanntid. Demonstratoren implementeres i første omgang på en standard PC-plattform.

En svært nyttig påbygning i demonstratoren vil være funksjonalitet for automatisk deteksjon og målfølging. En slik funksjon kan ha mange applikasjoner, der en bør tilpasse signalbehandlingen til hver spesifikk oppgave. Eksempler kan være deteksjon av båter for trafikkovervåkning i innseilinger og havneanlegg, inntrengingsalarm for oppdrettsanlegg og båtmarinaer, eller deteksjon av fugl for forskning på fuglers bevegelsesmønster.

Oppgaven går ut på å sette seg inn radar-signalbehandling med vekt på metodene som allerede er under utvikling i prosjektet, og metoder for etterbehandling av radarsignaler. Dernest skal det utvikles metoder for automatisk deteksjon av bevegelige mål basert på MTI behandlede radarsignaler. Metodene skal kunne skille ut mål fra clutter i et signalmiljø som er i stadig endring. Siden prosjektets teknologidemonstrator vil bli PC basert er det naturlig at også nye software komponenter utvikles på PC plattform, enten i MATLAB eller i et høynivåspråk. Metodene skal utvikles, implementeres, tilpasses og testes med reelle radarsignaler.

Oppgave utlevert: 24. Januar 2011

Veiledere: Morten Olavsbråten, IET, Yngve Steinheim, SINTEF IKT, og Erik Løvli, Radian AS

Abstract

In this thesis, methods for automatic detection for radar systems are investigated. The objective is to indicate the presence of targets in the midst of noise and clutter. One of the most efficent methods for doing this is to exploit the Doppler shift in reflections from moving targets. This is called Moving Target Indication (MTI), and it is used in many radar applications today. However, such functionality is not typical for radars employing a magnetron oscillator. The magnetron oscillator is widely used in civil marine radars, and MTI processing is of interest for such radars as well.

In addition to MTI processing, automatic detection may be applied in order to make decisions on target presence. This may be achieved by employing Constant False Alarm Rate (CFAR) detection and pulse integration. The challenges with automatic detection are prediction of the clutter power, and handling of non-homogeneous environments. Ideally, clutter components will be removed by the MTI process, leaving receiver noise and reflection from targets at the output. However, this is not necessarily the case when applied to a magnetron radar.

A particular automatic detector employing Ordered Statistics (OS) CFAR and binary pulse integration is investigated. This is a robust detector that may operate in the presence of multiple targets and non-Gaussian clutter. The binary integrator contributes in reducing the false alarm rate, such that acceptable performance may be achieved.

In order to find suitable parameters for the detector, analysis of an MTI processed radar signal containing reflection from waves at sea and a small boat is carried out. Also, the performance of the detector has been measured in terms of false alarm probability, and target detection. Analysis shows that Weibull or K-distribution are suitable models for the sea clutter, and that the MTI signal exhibits spatial correlation between clutter samples. The correlation is concluded to be the reason for degradation in performance, as detection on clutter appears as targets. Also, optimum parameters for the detector is found, and it is shown that increasing the number of reference samples increases the number of target detections.

Preface

This thesis is submitted in partial fulfillment of the requirements for the degree of Master of Science at the Department of Electronics and Telecommunications, Norwegian University of Science and Technology. It was written in the spring of 2011, and the assignment was given by Yngve Steinheim at SINTEF IKT and Erik Løvli at Radian AS. I would like to thank them for the numerous discussions on the subject and guidance in my work.

Trondheim, Norway, June 2011
Morten Ihlen

List of Abbreviations

CA	Cell Averaging
CDF	Cumulative Density Function
CFAR	Constant False Alarm Rate
IF	Intermediate Frequency
IID	Independent and Identically Distributed
MLE	Maximum Likelihood Estimation
MTI	Moving Target Indication
OS	Ordered Statistics
PDF	Probability Density Function
PRF	Pulse Repetition Frequency
SCR	Signal to Clutter Ratio
SNR	Signal to Noise Ratio

Contents

Chapter 1

Introduction

Radar is an instrument that is used for observing a natural environment, and detect physical objects herein. It employs electromagnetic waves to illuminate the environment, and receives echoes reflected by the objects. After reception, the received signal is processed before it is displayed to the user. The ability to detect objects at long distances, or in conditions of poor visibility, are key features of the radar. This is of particular importance for aircrafts and ships in order to navigate safely and avoid collisions. In the illuminated environment, numerous objects may introduce reflection and scattering of the transmitted radar signal, causing difficulties in detecting objects of interest. The objects of interest are usually termed as targets, and the interfering echoes are usually termed as clutter.

One method for detecting targets is to exploit the fact that targets often moves with larger velocities than clutter. A moving target will introduce a Doppler shift in the received signal, and with the use of Doppler filters, the slow moving clutter may be suppressed. This method is called MTI or Pulse Doppler processing, and it is dependent on knowledge of the transmitted frequency in order to measure the Doppler shift. This involves a stable oscillator and a high power amplifier in the transmitter circuit. However, requirements to size and long life time makes such transmitters expensive. An alternative to this is the magnetron power oscillator. The magnetron is a low cost and robust transmitter that is widely used in civil marine radars. However, because of the nature of the oscillator, each transmitted pulse starts at a random phase. This complicates the use of MTI filtering for these radars as the starting phase needs to be estimated for each pulse.

The work of Yngve Steinheim at SINTEF IKT and Erik Løvli at Radian AS on MTI processing for magnetron radars shows that this is possible, and it may be applied in practical radar systems [1]. This type of processing is often used in combination with automatic detectors, and it is of interest to develop such functionality for magnetron

radars as well. This may aid the human operator by indicating the presence of targets and their locations. The use of MTI processing and automatic detection for magnetron radars is a low cost solution that may be utilized in applications like ship radars, maritime coast surveillance, offshore ship surveillance, warning of snowy weather at airfields and research on birds.

One way of performing automatic detection this is to apply a pulse integrator and a threshold decision. The threshold may be derived using a Constant False Alarm Rate (CFAR) detector. The idea of such detectors is to provide an adaptive threshold and keep the false alarm rate constant. However, the correlation introduced by the pulse integrator increases the complexity for theoretical analysis. Prior to this thesis, the author wrote a project paper on non-coherent pulse integration as a part of an automatic detector [2]. This has been set aside due to the increased complexity in using pulse integration prior to CFAR detection. In the search for other solutions, a detector containing an Ordered Statistics (OS) CFAR followed by a binary integrator has been found. For this configuration, theoretical CFAR is not only obtained for the CFAR detector, but it is also conserved through the pulse integrator stage. This makes it tractable for use in practice.

The thesis consists of two stages. First, an MTI processed radar signal is analysed in order to reveal statistical properties of the clutter components. The purpose of this is to find statistical models that may be used for prediction of the adaptive threshold. Secondly, the detector will be tested on the MTI signal, and the performance in terms of false alarm probability and target detection will be evaluated in order to find suitable parameters for the detector.

Chapter 2

Theory

The radar is a system that is used for detecting presence, range, speed and direction of physical objects by transmitting electromagnetic waves, and record the reflections. If the transmitted signals are pulses rather than a continuous wave, the radar may use the same antenna for transmission and reception of the signal. After reception, signal processing needs to be applied in order to extract information of the objects. The main components in a radar system are a transmitter, a receiver and an antenna. There are various aspects to the design of each system block, which is dependent on the purpose of the particular radar. In Figure 2.1, some principal system blocks of a radar using magnetron transmitter is shown.

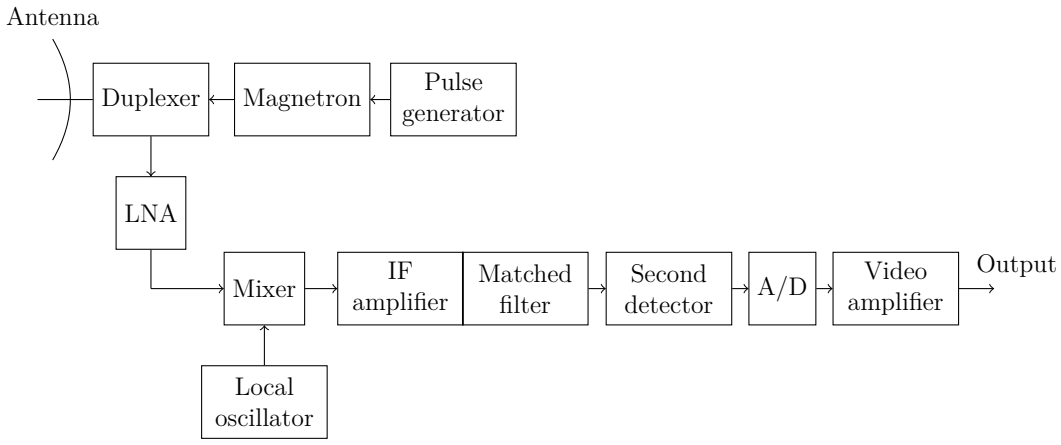

Figure 2.1: A pulsed radar system employing magnetron transmitter.

The duplexer performs the swithcing operation between transmission and reception. The received signal is amplified by a Low Noise Amplifier (LNA) before it is converted to Intermediate Frequency (IF). After amplification and mathed filtering the

amplitude or power is calculated by the second detector. This is usually termed as linear or square-law detection. The output of the second detector may be sampled before it is displayed to the user. MTI and automatic detection may be applied after the matched filter. MTI utilizes the phase information, and automatic detection utilizes the magnitude. In this chapter, a brief introduction to radar theory and automatic detection will be presented. Some understanding of the illuminated environment, and its influence on the reflected radar wave will be discussed. In particular, a discussion on sea clutter is provided since this is the type of clutter that will be analysed. Also, the concept of MTI processing will be shown as it is mentioned frequently in this thesis. The methods of CFAR detection will be shown in detail, and two CFAR detectors will be discussed. Also, statistical models for prediction of the CFAR multiplier, and theory on binary integration will be presented.

2.1 Signal Model

In this section, a simple signal model will be presented in order to define the received components. In general, the received pulses contains signal energy reflected from any scatterer within the range of the radar and additive white Gaussian noise. The received power may be written as,

$$P_r = P + P_w, \tag{2.1}$$

where P is reflected power from any scatterer and P_w is the power of white Gaussian noise. A scatterer is any object that intercepts and reflects the transmitted radar signal, including waves at sea, terrestrial objects and percipitation. The latter is commonly termed sea-, land- and rain clutter. Thus, P_r may be expanded to,

$$P_r = P_s + P_c + P_w, \tag{2.2}$$

where P_s is reflected power from targets and P_c is reflected power from clutter. Clutter often exhibit reflections of large magnitude, and tend to mask targets on the radar display. For surface clutter, the received clutter power for small grazing angles is given as,

$$P_c = \frac{cP_tG^2\lambda^2\tau\theta_B\sigma^0}{2^7(\pi R)^3}. \tag{2.3}$$

The latter is derived from the radar equation, and its shown in Appendix A. At short ranges, one may assume that $P_c >> P_w$ and P_w may be neglected. However, as seen by equation (2.3), the received clutter power is reduced as the range R increases, and at long ranges the assumption becomes invalid. For simplicity, the two components will be treated as one in this thesis, and it will be referred to as clutter. Thus, the reviewed model is,

$$P_r = P_s + P_n, \tag{2.4}$$

where P_n is the received power reflections from clutter plus noise. For target detection, knowledge of the clutter statistical properties is necessary, and it will be given much attention in this thesis. Therefore it is important to emphasize that when received radar signals are investigated, the clutter is actually equal to clutter plus noise. In the next section, the characteristics of sea clutter is described.

2.2 Sea Clutter

Sea clutter is a term for radar reflections made by waves on the sea surface. Waves at sea are a complex phenomena influenced by different parameters, such as wind speed, currents and topology of the sea bottom. As detection of targets at sea is the objective, a brief introduction on sea clutter and its complexity will be given in this section. Also, the effects of operating at low grazing angles will be discussed. In general, the sea may be assumed to consist of two components: a slow varying sea swell and rapid varying ripples. The ripples are associated with roughening of the sea surface in a small area caused by local wind. They will act as a number of different scatterers reflecting the incoming radar wave in different directions, creating interference in the backscattered signal. The interference component of the backscattered signal is commonly termed speckle. If a patch on the sea surface is observed over time, it may be seen that the mean level of the amplitude varies. This is caused by the long sea swell that arises from different mechanisms as those mentioned in the beginning of this section. Ripples are also a contributor to the sea swell in areas with large wind speeds. If the radar is at a high grazing angle, and the resolution cell is greater than the sea swell wavelength, the amplitude of the clutter may be modelled as just speckle. This is known to be Rayleigh distributed. Furthermore, observation of small targets requires the received pulses to have a relatively short decorrelation time. This is acheived at high grazing angles if the radar employs frequency agility. Frequency agility is the operation of changing the transmitted frequency by $\Delta f \geq B$ for each pulse. Thus, the phase shifts between

pulses are $\Delta\phi \geq 2\pi$, where $\Delta\phi = 2\pi\Delta f/B$ and B is the bandwidth. In range, the decorrelation time is mainly dependent on the pulse length. On the other hand, if the grazing angle and the resolution cell are decreased, the probability of observing large clutter amplitudes increases. This is the case for shipborne radars, as the illuminated range is much larger than the height of the radar placement. Thus, the distribution of the observed amplitudes will have a longer tail than the Rayleigh distribution, and the clutter will become more spiky. In addition, the decorrelation time increases in spite of the use of frequency agility. This is due to the variation in mean introduced by the long sea swell. Experiments have shown that the variable mean level is best modelled by the Gamma distribution, which gives rise to the compound K-distribution [3] [4]. This model will be presented in Section 2.6.4. In the next section, the concept of MTI processing is presented.

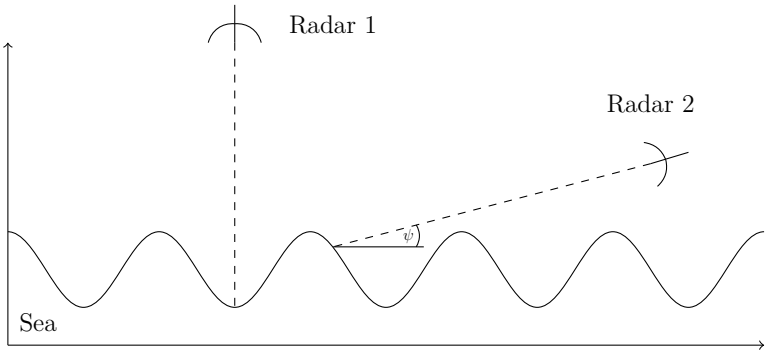

Figure 2.2: Radar 1 and Radar 2 is at high and low grazing angle ψ, respectively.

2.3 Moving Target Indication

In many radar scenarios, the reflection from clutter complicates the detection of targets. Clutter may exhibit large magnitudes, while the target cross section is unaltered. Reflections from clutter can be as much as 60-70 dB larger than target echoes [5, p.105]. In principle, clutter behaves similarily to any other object that may intercept the transmitted radar signal. To distinguish targets from clutter it is necessary to look at properties that are unique for targets. In many situations, targets have a larger relative velocity to the radar than the stationary or slow moving clutter. This may be utilized since moving targets will cause shifts in the Doppler frequency of the reflected signal. For a two-way propagating radar antenna, the shift in the received Doppler frequency is given as,

$$f_d = \frac{2v_r}{\lambda_c}, \tag{2.5}$$

where v_r is the radial velocity of the target, and λ_c is the transmitted wavelength. If a Doppler filter is used to suppress slowly moving clutter, detection of targets with larger velocities may be eased. The principle is illustrated in Figure 2.3. The drawback with using a single Doppler filter is that the frequency response is zero at the Pulse Repetition Frequency (PRF), and its harmonics. Thus, targets that reflect Doppler shifts at these frequencies will be suppressed. The corresponding velocities are usually termed as blind speeds. MTI or Pulse Doppler processing are widely used in radar applications, such as military air-defense radars and civil air-traffic control radars. For ground applications one should be aware that stationary targets and targets at low v_r will be rejected by the Doppler filter. Thus, detection of ground targets at all velocities should not rely entirely on MTI or Pulse Doppler processing. Nevertheless, this concept aids in the process of detecting targets [6] [5] [7]. In the next section, the principle of adaptive thresholding is presented.

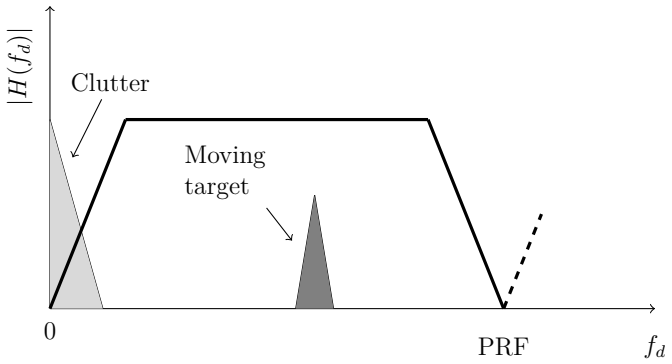

Figure 2.3: Concept of MTI. Moving targets are assumed to have larger velocities than clutter, and a Doppler filter may be used for suppression. The unambigious Doppler frequencies are $0 \leq f_d \leq \text{PRF}$.

2.4 Adaptive Thresholding

Detection of targets in radar signals involves comparing the linear or square-law detected signal to a threshold. If the signal magnitude crosses the threshold, a target may be declared present. However, in a clutter environment with large clutter spikes, the clutter will occasionally cross the threshold and falsely be declared as targets. These events are termed as false alarms, and its frequency is dependent on the setting of the threshold. This is a key element in target detection and will be discussed extensively in this thesis. In this section, an introduction to the concept of adaptive thresholding is given. The objective of the threshold is to detect targets, but it should also minimize the number of false alarms. Ideally, all targets should

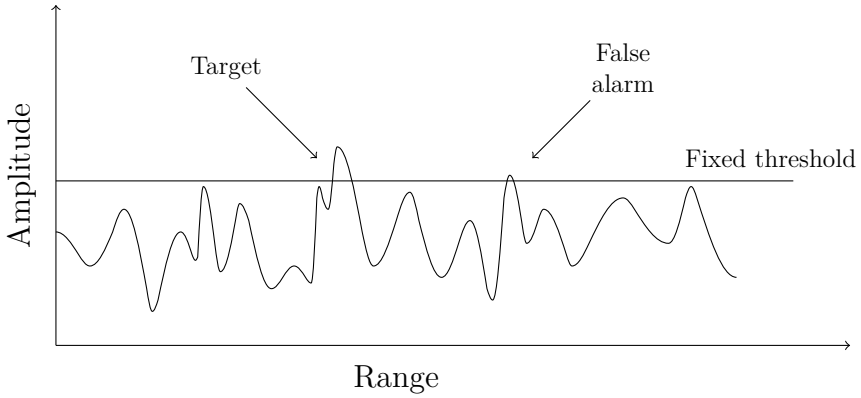

Figure 2.4: Received pulse compared to a fixed threshold

be detected and no false alarms should occur. A fixed threshold and received signal amplitude is shown in Figure 2.4. Increasing the threshold will reduce the probability of falsely detecting clutter reflections, but it also reduces the probability of detecting targets that reflect small amounts of signal energy compared to the clutter. That is, targets with small Signal to Clutter Ratio (SCR). As it is desired to detect as many targets as possible, the threshold often needs to be set at a level where false alarms are unavoidable. Thus, higher detectability is achieved on the expense of higher false alarm rate. To find suitable threshold values, a common approach is to try to control the probability of false alarms, P_{fa}. In this manner, the threshold can be set according to the false alarm tolerance of the application. The calculation of a fixed threshold implies that all possible clutter values need to be known a priori if an overall P_{fa} is to be obtained. In practice, the clutter environment might change over time and the local P_{fa} will vary. Also, the knowledge of all possible clutter values is difficult to obtain. Thus, it may be more tractable to adapt the threshold to the current clutter environment and obtain a local P_{fa}. If a local P_{fa} is maintained by adjusting the threshold, the overall P_{fa} will also be maintained. In addition, by adjusting the threshold the probability of detecting targets with small SCR will increase compared to the fixed threshold. In most cases, setting an adaptive threshold involves measuring the local clutter mean level [4]. As described in Section 2.2, the mean level of sea clutter varies due to long sea swells. To be somewhat coherent with this variation, a set of received values in the range direction may be used to estimate the local mean value at each range instance of a received pulse. This concept is utilized in a class of detectors that is termed CFAR detectors. The operation of such detectors will be discussed in the next section.

2.5 CFAR Detection

CFAR detection is a term for methods that generate adaptive thresholds, and maintains a constant probability of false alarm. Consider a fixed threshold in a clutter environment with varying clutter mean level. In this case, the false alarms will be dependent on the mean, as threshold crossings are more likely to occur in regions with high mean. This may be avoided by using CFAR techniques, and their general operation will be presented in this section. The purpose of CFAR is to maintain P_{fa} both locally and globally. The idea is to employ a sliding window consisting of $N/2$ reference cells in front of and behind the cell under test, as shown in Figure 2.5. The cell under test may be denoted by a random variable Y, and the reference cells may be denoted by random variables X_i, where $1 \leq i \leq N$. Values in the reference cells are used to calculate an estimate of the clutter mean. After estimation, the local threshold value T is to be obtained. This is done by multiplying the estimated mean with some scaling factor α, and it is derived from a statistical distribution model fitted to the amplitude or power of the clutter. α is commonly termed as the CFAR multiplier. Finally, a decision rule is applied to determine whether a target is present or not. It may be given as the following hypothesis test [8],

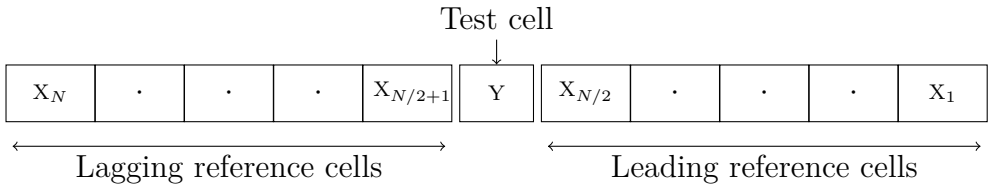

Figure 2.5: The reference cells X_i are located in front of and behind the test cell Y, where $1 \leq i \leq N$.

$$\text{Decision} = \begin{cases} H_0\text{: no target present,} & \text{if } Y < T \\ H_1\text{: target present,} & \text{if } Y > T. \end{cases}$$

Such a decision rule may be realized by using a binary quantizer, which will be described further in Section 2.8. α is usually calculated for a predetermined value of P_{fa}. The relation between the two parameters involves the probability distribution of the clutter statistics. This will be described in detail in Section 2.6, but it is worth noticing that in literature, a detection method is said to be CFAR if the relation between α and P_{fa} is independent of the true clutter statistics. That is, the method is guaranteed to provide a constant false alarm rate. The difference between CFAR methods is how the mean estimate is obtained. Two such methods will be presented in this thesis, and it is convenient to start with the Cell Averaging (CA) CFAR.

2.5.1 CA CFAR

The CA CFAR method is frequently mentioned in theory and it is often used as reference when investigating other CFAR methods. This is because it provides the maximum detection probability P_d in homogeneous backgrounds if the clutter environment is Exponential distributed. Also, it requires the values in the reference cells to be independent and identically distributed. In this section, the CA CFAR method will be presented along with some of its properties. The operation is to calculate the average of the values in the reference cells and multiply with α. That is,

$$T = \alpha \left(\frac{1}{N} \sum_{i=1}^{N} X_i \right), \tag{2.6}$$

where X_i is the i'th reference cell. In addition, guard cells are employed in front of and behind Y. This is to prevent the threshold to rise due to target energy located outside Y. A block diagram of the CA CFAR method is shown in Figure 2.6. As mentioned, this method works well when the clutter is homogeneous. However, when the clutter is non-homogeneous, the performance may be degraded. Non-homogeneous environments occur when a clutter edge is present or when targets are closely located in range.

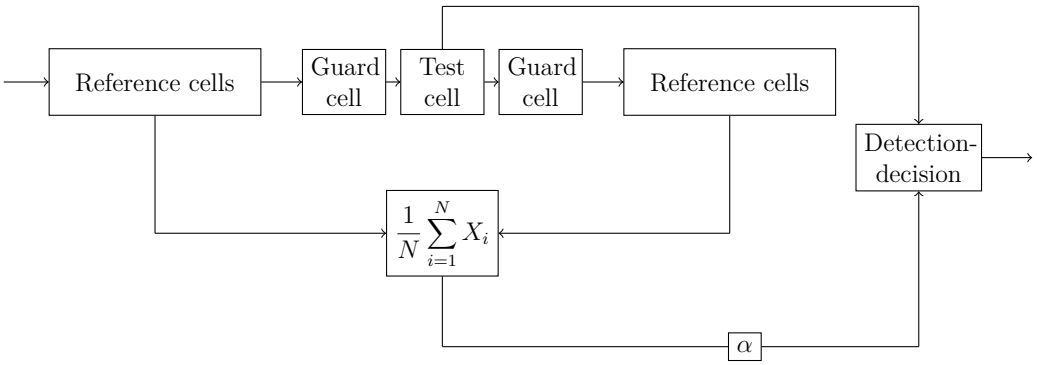

Figure 2.6: The CA CFAR scheme. The threshold is derived by averaging the N reference cells, and multiply with the CFAR multiplier α. Y is then compared to the threshold to make a decision on target presence.

A clutter edge is a rise in the local mean value, and may occur when e.g. rain or snow is present in parts of the reference cells. This will result in rising the threshold, and targets in the low clutter region may not be detected. Also, when values in the high clutter region are evaluated in Y, false alarms will occur. This is due to the low clutter values still included in the reference cells, contributing to a threshold that

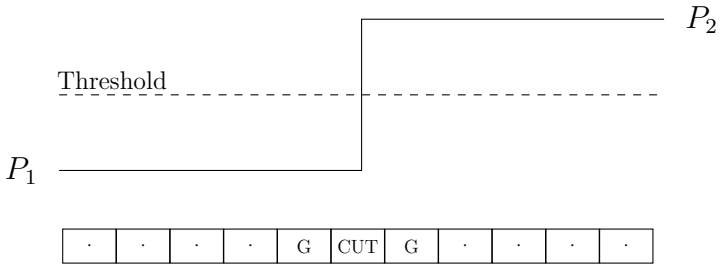

Figure 2.7: P_1 and P_2 represents the mean values in the low and high clutter regions, respectively

is too low. The principle of a clutter edge is shown in Figure 2.7. For the situation where targets are closely located in range, target masking may occur. In general, when a target is present, the threshold will rise significantly in front of and behind the target. If other targets are located in these areas, they may not be detected. In addition, large N will yield better estimates of the mean value, but it is on the expense of the detectors adaptability [9]. To combat these problems, numerous CFAR methods has been invented. In the next section, one of these methods will be presented and compared to the CA CFAR method.

2.5.2 OS CFAR

OS CFAR was proposed in 1983 by Rohling [10]. The goal was to combat the problems related to the operation of CA CFAR in non-homogeneous environments. In this section, this method will be presented along with a comparison to the CA CFAR method. The idea of OS CFAR is to order the values in the reference cells, and choose one of them as an estimate of the clutter level. Assume a number of reference cells surrounding Y, denoted $X_1, X_2, ..., X_N$. The k'th largest value is denoted $X_{(k)}$, and is chosen as the representative for the local clutter level. To find $X_{(k)}$, the values in the reference cells need to be sorted such that,

$$X_{(1)} \leq X_{(2)} \leq \cdots \leq X_{(N)}, \tag{2.7}$$

where $X_{(1)}$ and $X_{(N)}$ is the smallest and largest of the X_N values. The threshold is derived by multiplying $X_{(k)}$ with α, such that,

$$T = \alpha X_{(k)}. \tag{2.8}$$

A block diagram of the OS CFAR is shown in Figure 2.8. This method does not

require guard cells since clutter amplitudes outside $X_{(k)}$ does not affect the calculation of the threshold. By doing this, the problems related to clutter edges and interfering targets may be reduced. However, the performance will be limited by the choice of k. Obviously, choosing $k = N$ will ensure conservation of the false alarm rate, but target detection will be impossible. According to reference [10], k should be chosen to be larger than $N/2$ in order to to avoid false alarms when encountering clutter edges. This implies that the threshold will be increased before clutter edge values enters Y, and stay at high clutter level estimates longer than the duration of the clutter edge. Thus, the estimated mean will be extended in range compared to the true clutter.

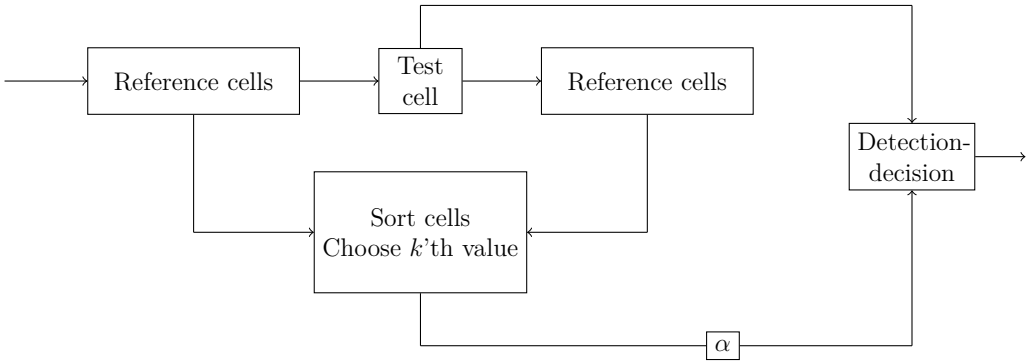

Figure 2.8: The OS CFAR scheme. Thresholds are derived by sorting the N reference cells and choosing the k'th largest value. The sorted value $X_{(k)}$ is multiplied with the CFAR multiplier α before comparison with Y.

Also, when high clutter values appears in less than $N - k$ cells, false alarms may occur [9]. Regarding the situation of multiple targets, $N - k$ should not be less than twice the extension of one target in range. Otherwise, two targets of equal magnitude will both be masked if they are present in the sliding window simultaneously. In reference [11] a more general definition is given. It states that if there are J number of targets present in the reference cells, the threshold will not rise extensively as long as $J \leq N - k$. Moreover, in reference [10] it is shown that $k = 7N/8$ is closest to the CA CFAR threshold in homogeneous situations when $N = 24$. However, it is recommended to use $k = 3N/4$ in order to reduce the distance between the rise of the threshold and the clutter edge. Also, for OS CFAR it is possible to operate with large values of N for increased estimation accuracy without compromising the adaptability of the detector. Several other CFAR techniques has been proposed such as the Greatest Of CFAR, Smallest Of CFAR, Trimmed Mean CFAR, and Censored Ordered Statistics CFAR. The techniques exhibit properties that are advantageous in various clutter situations. However, in this thesis the discussion is limited to the CA and OS CFAR. In the next section, the derivation of the CFAR multiplier for

OS CFAR will be presented.

Table 2.1: Advantages and disadvantages in using CA and OS CFAR.

Method	Advantages	Disadvantages
CA CFAR	Homogeneous clutter: Maximizes P_d if the samples are iid.	Clutter edge: Degrades P_d and increases the number of false alarms. Multiple targets: Masking of closely located targets.
OS CFAR	Clutter edge: No increase in P_{fa} if the range of the increased mean is larger than $N-k$. Multiple targets: Can resolve $J = N-k$ target cells independent of the target locations	Homogeneous clutter: Loss in P_d compared to CA CFAR.

2.6 CFAR Multiplier

In this section, the derivation of the CFAR multiplier α for OS CFAR will be given. The procedure is to solve the equation for P_{fa} and extract α. For most CFAR methods, P_{fa} is a fixed value, and given as a part of the design. Y takes values from the clutter Probability Density Function (PDF). The probability of Y taking a value which is larger than a threshold T is denoted the probability of false alarm. That is,

$$P_{fa} = P(Y \geq T) = \int_T^\infty p(y)\, dy, \tag{2.9}$$

where $p(y)$ is the clutter PDF. The principle is shown in Figure 2.9, where P_{fa} is equal to the shaded area. As mentioned in Section 2.5.2, the threshold value for OS CFAR is given by $T = \alpha X_{(k)}$. Where $X_{(k)}$ is the random variable in the reference cell that has the k'th largest value. Inserting this in equation (2.9) yields,

$$P_{fa} = P(Y \geq \alpha X_{(k)}). \tag{2.10}$$

To solve this equation, the statistics of both $X_{(k)}$ and Y need to be included. The values in the test cell Y is taken from the same set of data as X. Thus, they have the same distribution. The value of $X_{(k)}$ is taken from a set of N values in the reference window, and the probability of the k'th largest value yields the binomial distribution. It is given as,

$$p(X_{(k)}) = p_k(x) = k\binom{N}{k} p(x)P(x)^{k-1}(1 - P(x))^{N-k}, \tag{2.11}$$

where $p(x)$ and $P(x)$ is the PDF and CDF of X, respectively. Derivation of this equation is given in appendix D. Now, equation (2.10) can be written as,

$$P_{fa} = \int_0^\infty P(Y \geq \alpha x) p_k(x)\, dx. \tag{2.12}$$

Solving equation (2.12) with a fixed P_{fa} gives the desired α. This will be shown for several models in the proceeding sections. Obviously, the clutter statistics need to be known a priori to find the CFAR multiplier for a given false alarm rate. This implies that for practical applications, different statistical models need to be evaluated to obtain the best performance. In the following sections, the distributions investigated in this thesis is presented.

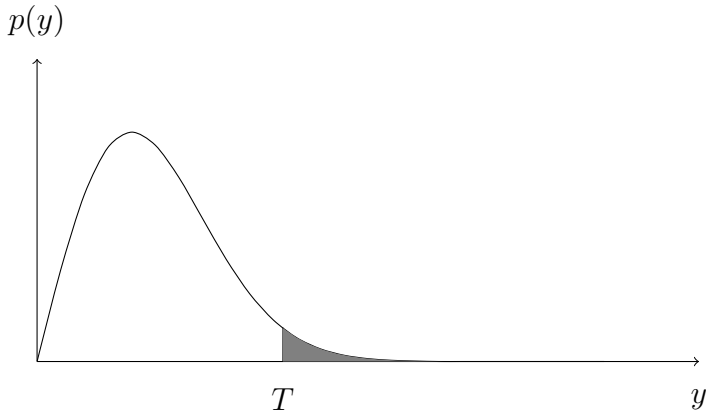

Figure 2.9: The concept of probability of false alarms. The y-axis represents the probability $p(y)$ of observing a value y. The probability of observing values larger than T is equal to the area of the shaded region.

2.6.1 Exponential Distribution

A high resolution radar illuminating an area from a high grazing angle will observe a number of individual scatterers. The in-phase (I) and quadrature (Q) components in the reflected complex signal from the scatterers are observed to be Gaussian distributed [5, p.37]. The absolute value of two Gaussian distributed components yield Rayleigh distribution, and its PDF is given by,

$$p(x) = \frac{2x}{\bar{z}} \exp\left(-x^2/\bar{z}\right), \tag{2.13}$$

where $\bar{z}$ is the second moment of x. That is,

$$\bar{z} = E(x^2) = \sum_x x^2 p(x), \tag{2.14}$$

where E denotes the expectation value. If the signal is square-law detected, the power, $z = x^2$, is distributed by the Exponential distribution. The PDF and the Cumulative Density Function (CDF) is given by,

$$p(z) = \frac{1}{\bar{z}} \exp(-z/\bar{z}), \tag{2.15}$$

and,

$$P(z) = 1 - \exp(-z/\bar{z}), \tag{2.16}$$

respectively. $\bar{z}$ is now the mean value (or first moment) of z, and $z \geq 0$ [5, pp.436 – 437] [12, p.220]. Inserting equation (2.15) and (2.16) in equation (2.12) gives P_{fa} for Exponential distributed clutter or noise. That is,

$$P_{fa} = \frac{1}{\bar{z}} \binom{N}{k} \int_0^\infty \exp\left(\alpha z/\bar{z}\right) \left[\exp(-z/\bar{z})^{N-k+1}(1 - \exp(-z/\bar{z}))^{k-1}\right] dz. \tag{2.17}$$

In reference [10] it is shown that the solution to this integral is,

$$P_{fa} = \frac{N!(\alpha + N - k)!}{(N-k)!(\alpha + N)!}. \tag{2.18}$$

The last expression is not dependent on the mean clutter power $\bar{z}$. Thus, with this distribution the method may guarantee CFAR. The performance of OS CFAR when

applying an Exponential distribution has been investigated in reference [11]. It was shown a detection loss of approximately 3 dB compared to the ideal fixed threshold when $N = 16$, $k = 10$ and $P_{fa} = 10^{-5}$. Rayleigh or Exponential distribution may be good models if the CFAR multiplier is to be calculated for the speckle component or receiver noise only. However, as discussed in Section 2.2 the reflections from sea clutter at low grazing angles exhibit longer tailed distributions than those presented here. Hence, calculating the CFAR multiplier for such distributions need to be investigated, and is presented in the next sections.

2.6.2 Weibull Distribution

In this section, the Weibull distribution is presented. The Weibull PDF is a two parameter distribution, and it is able to model data with longer tails than the Rayleigh distribution. The two parameters are the shape parameter C and the scale parameter B. The Weibull PDF for amplitude values is,

$$p(x) = \frac{C}{B}\left(\frac{x}{B}\right)^{C-1} \exp\left(-\left(\frac{x}{B}\right)\right)^{C}, \tag{2.19}$$

where $C > 0$ and $B > 0$. Decreasing C increases the tail of the PDF, and for $C = 2$ the expression is equal to the Rayleigh distribution. The CDF of the Weibull distribution is given as,

$$P(x) = 1 - \exp\left(-\left(\frac{x}{B}\right)\right)^{C}. \tag{2.20}$$

If it is assumed that the clutter encountered is Weibull distributed, equation (2.12) must be solved to obtain the CFAR multiplier. In reference [13], it is shown that the solution to this is given by,

$$P_{fa} = \frac{N!(\gamma^C + N - k)!}{(N-k)!(\gamma^C + N)!}, \tag{2.21}$$

where γ is the multiplier and $\gamma = \alpha^{1/C}$. For square-law detected samples, $z = x^2$, the threshold multiplier is obtained by simply squaring $\alpha^{1/C}$. That is,

$$\gamma = \alpha^{2/C}. \tag{2.22}$$

It should be noticed that the method is only CFAR if C is known a priori. If not, C needs to be estimated and CFAR cannot be guaranteed. In reference [14], a method

using two of the ordered samples in the reference window was proposed. The method obtains CFAR if C is unknown. This method was investigated and compared to equation (2.21) when $C = 2$ in reference [13]. The results for the latter showed that the smallest detection loss was 2.3 dB compared to a fixed threshold when C was known a priori. For unknown C, the two ordered samples method showed a detection loss of 9.4 dB. This loss was observed when parameters were chosen such that the algorithm had no immunity to interfering targets. From the results, it was concluded that it is better to use equation (2.21) and assume $C = 1.5$ if the uncertainty is $1.5 \leq C \leq 2$. Also, if the CFAR is to have immunity against interfering targets, equation (2.21) was concluded to be a better choice than the two ordered samples method. Equation (2.21) was also tested by in reference [15] for $C = 1$. The results showed that the detection loss was 3.4 dB for a non-fluctuating target and 3.1 dB for a Swerling case 2 target. The Swerling target models are presented in appendix C. In the next section, the Log-Normal distribution is presented.

2.6.3 Log-Normal Distribution

The Log-Normal distribution is a long tailed distribution, and may be used to model clutter where large values occur more frequently. It is also the most heavy tailed distribution presented in this thesis, and it has been said that it tends to predict too high tails compared to what is observed in measured data [5, p.438]. If the signal is square-law detected the PDF may be written as,

$$p(x) = \frac{1}{\sqrt{2\pi s^2} z} \exp\left(-\frac{1}{2s^2}\left(\ln\frac{z}{z_m}\right)^2\right), \tag{2.23}$$

where s^2 is the variance of $\ln(x)$, and z_m is the median value of z. The median value is related to the mean by $z_m = e^{\mu}$, where μ is the mean value of $\ln(z)$. The CDF is given by,

$$P(z) = \frac{1}{2}\text{erfc}\left(\frac{\ln(z) - \mu}{\sqrt{2}s}\right), \tag{2.24}$$

where $\text{erfc}(\cdot)$ is the complementary error function, and it is given by,

$$\text{erfc}(x) = \frac{2}{\sqrt{\pi}} \int_x^{\infty} e^{-t^2}\, dt. \tag{2.25}$$

The value of P_{fa} may be solved with numerical integration if equation (2.23) and (2.24) are inserted in equation (2.12). Again, this is not CFAR if μ and s need to be

estimated, since equation (2.21) will be dependent on the distribution parameters. If CFAR is to be obtained, the method in reference [14] may be used. In reference [16] it was found that when $N = 16$, the detection loss was 4.14 dB and 10.3 dB for $s = 0.5$ and $s = 1$. For $N = 32$, the detection loss was 2.3 dB and 5.58 dB for the same values of s. However, the parameters of the CFAR was set to have no immunity against interfering targets. In the next section, the K-distribution is presented.

2.6.4 K-Distribution

As described in Section 2.2, the sea clutter may be viewed upon as a Rayleigh distributed speckle and a Gamma distributed mean level. Combining the two distributions yield the compound K-distribution. This was proposed for modeling sea clutter by Jakeman and Pusey in 1976 [17], and further investigation has been carried out by Watts et al. [18] [3] [4]. This is the only model that is based on some physical understanding of the sea structure. The Rayleigh distribution was given in equation (2.15), and the Gamma distribution may be given as,

$$p(\bar{z}) = \frac{b^v}{\Gamma(v)} \bar{z}^{\,v-1} e^{(-b\bar{z})}, \qquad 0 \leq \bar{z} \leq \infty, \tag{2.26}$$

where b is the scale parameter, and v is the shape parameter. The K-distribution is obtained by averaging the Rayleigh distributed speckle component over all possible values of $\bar{z}$. That is,

$$p(x) = \int_0^\infty p(x|\bar{z}) p(\bar{z})\, d\bar{z}, \tag{2.27}$$

where $p(x|\bar{z})$ is the Rayleigh PDF with its dependency on the varying mean emphasized. The derivation of the PDF and CDF of the K-distribution is shown in appendix E. The resulting PDF for linear detected values is,

$$p(x) = \frac{4b^{\frac{(v+1)}{2}} x^v}{\Gamma(v)} K_{v-1}(2\sqrt{b}x), \tag{2.28}$$

where K_{v-1} is the modified Bessel function of second kind. The CDF is given as,

$$P(x) = 1 - \frac{2b^{v/2} x^v}{\Gamma(v)} K_v(2\sqrt{b}x). \tag{2.29}$$

For square-law detected values ($z = x^2$) the PDF and CDF may be given as,

$$p(z) = \frac{2b^{\frac{v+1}{2}} z^{\frac{v-1}{2}}}{\Gamma(v)} K_{v-1}(2\sqrt{bz}), \tag{2.30}$$

and

$$P(z) = 1 - \frac{2(bz)^{v/2}}{\Gamma(v)} K_v(2\sqrt{bz}). \tag{2.31}$$

For OS CFAR operation, numerical integration must be applied in order to solve equation (2.12). Since the expression is dependent on estimates of the statistical parameters, the method cannot guarantee CFAR. The use of OS CFAR in K-distributed clutter has been investigated in reference [19]. The results show that CFAR detectors, in general, are more sensitive to spiky clutter (small v) in terms of detection probability. However, increasing the number of reference cells N will reduce the loss. For $N = 32$, $k = (3/4)N$ and $P_{fa} = 10^{-6}$, the CFAR loss was shown to be in the region 1.45 dB - 17.33 dB when v varied from 9.5 to 0.1. Also, the results show that CA CFAR performs better than OS CFAR in terms of CFAR loss, particularly for small values of v. The effect of having partially correlated mean levels are also investigated. This is of interest as it is a more realistic assumption in practical applications. The conclusion from this was that detection loss for most degrees of partial correlation in the mean level was close to that of completely uncorrelated mean level. In the next section, the MLE method for estimating distribution parameters is presented.

2.7 Maximum Likelihood Estimation

When the parameters of different distributions are unknown, maximum likelihood estimation (MLE) may be employed. The method assumes the parameter θ to be in the set Θ, and calculates the joint probability of a set of data x_1,x_2,...,x_n for various choice of θ. If the data is Independent and Identically Distributed (IID), the joint PDF may be written as [12],

$$p(x_1, x_2, ..., x_n|\theta) = \prod_{i=1}^{n} p(x_i|\theta). \tag{2.32}$$

Taking the logarithm on each side of the expression yields,

$$\ln(p(x_1, x_2, ..., x_n|\theta)) = \sum_{i=1}^{n} \ln(p(x_i|\theta)). \tag{2.33}$$

The last expression is referred to as log-likelihood, and the objective is to find the parameter θ which maximizes equation (2.33). Thus, the estimated parameter may be written as,

$$\hat{\theta} = \arg\max_{\theta \in \Theta} \frac{\ln(p(x_1, x_2, ..., x_n|\theta))}{n}. \tag{2.34}$$

To obtain the correct parameters for different distributions, the data needs to be uncorrelated. From the previous discussion on sea clutter, this may be obtained for radar signals recorded at high grazing angles with frequency agility employed. However, at low grazing angles the clutter will appear more spiky and neighboring pulses may be correlated. This is due to the slowly varying mean level of the clutter. However, the speckle will still be uncorrelated. In these circumstances, statistical independency may be obtained by taking data from cells separated with more than the decorrelation distance [20]. In the next section, the theory on binary integrator will be introduced.

2.8 Binary Integrator

The binary integrator is a detector that may be used as a second threshold for detecting targets. Due to its simplicity and robustness in non-Gaussian clutter, it has been widely used in radar detectors since the 1950's. In this section, the theory and operation of the binary integrator will be presented. Assume n pulses are received by the radar as it scans past a target. After range sampling, detection and thresholding, a decision rule is applied. As described in Section 2.5, the hypothesis H_1 will be declared if a target is present and H_0 otherwise. The decision rule may be realized with a binary quantization process, where each range sample in the received pulse is compared to the threshold of the first detection process (e.g. a CFAR detector). If the magnitude of a range sample exceeds the threshold, the quantizer will produce a 1 at the output. If the magnitude is below the threshold, the quantizer will produce a 0. Thus, each pulse is converted into a binary vector containing detections after the first thresholding. After processing n pulses into binary vectors, the binary integrator may carry out its operation. At each range instance, the number of 1's in the n pulses will be counted and compared to a predetermined value m, where $1 \leq m \leq n$. If at least m of the n samples contains 1's a target is detected. Hence, m may be viewed as a threshold itself. Assume the probability of detecting exactly m 1's out of n samples. The probability of success is given by,

$$P_d(M = m) = \binom{n}{m} p_d^m (1 - p_d)^{n-m}, \tag{2.35}$$

where M is a random variable denoting the number of successes, and p_d is the probability of detecting a 1 in each sample. The probability of having at least m successes yields the sum of $n - m$ Bernoulli trials. That is [21, pp.338 – 342],

$$P_d(M \geq m) = \sum_{i=m}^{n} \binom{m}{i} p_d^i (1 - p_d)^{n-i}. \tag{2.36}$$

Similarly, the probability of false alarms at the output of the binary integrator is obtained by inserting the single pulse P_{fa} after the first thresholding. This results in,

$$P_f(M \geq m) = \sum_{i=m}^{n} \binom{n}{i} P_{fa}^i (1 - P_{fa})^{n-i}. \tag{2.37}$$

The loss in signal to noise ratio (SNR) by using binary integrators has been reported to vary between 1 dB to 2.5 dB, given that the optimum m is chosen [5, p.293]. Several studies have been devoted to studying the optimum m. In reference [22] it is found that for certain ranges of n, the optimum m may be given by,

$$m_{\text{opt}} \approx 10^b n^a, \tag{2.38}$$

where a and b are coefficients that depend on which Swerling model the target represents. The coefficients are given in Table 2.2. It was also found that the choice of m can vary around m_{opt} without significant loss in SNR. The value of n is related to the number of received pulses containing reflections from a target within the 3 dB beamwidth n_b. In reference [23], it is shown that the optimum number of pulses that should be integrated is,

$$n = 0.84 n_b, \tag{2.39}$$

when the antenna pattern is Gaussian shaped and no weighting of the received pulses is applied. If the pulses are weighted the integration loss is reduced by 1.6 dB. The binary integrator is said to robust because the actual energy of clutter detections will not affect the performance. Moreover, the binary integrator has the same performance in high-resolution non-Gaussian clutter as in Gaussian noise in terms of eliminating noise or clutter components that may contribute to false

alarms [5, pp.292 – 294]. It should be stressed that equation (2.36) and (2.37) also assume independent and uncorrelated samples. This may be preserved for high-resolution radars employing frequency agility as mentioned in Section 2.2. The performance in non-Gaussian clutter has shown excellent performance [7, pp.7.7 – 7.11]. This, along with its simplicity, may explain its popularity in radar systems encountering long tailed noise or clutter. In the next chapter, the automatic detector investigated in this paper will be presented. Analysis of an MTI processed radar signal is carried out in order to provide reasonable parameters for the detector. Also, expected theoretical performance will be shown for comparison with the results in Chapter 4.

Table 2.2: Parameters for equation (2.38) taken from reference [22]

SW	a	b	Range of n
0	0.8	-0.02	5-700
1	0.8	-0.02	6-500
2	0.91	-0.38	9-700
3	0.8	-0.02	6-700
4	0.873	-0.27	10-700

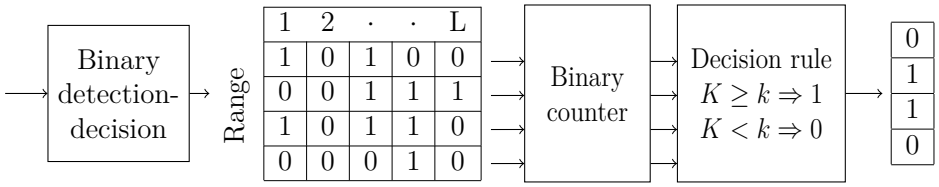

Figure 2.10: The operation of a binary integrator for one set of $n = 5$ trials and $m = 3$. The output vector indicates success or failure at each range instance.

Chapter 3

Method

The objective of this thesis is to design an automatic detector for radar signals after MTI processing. It is to work on radar signals received by a seaborne radar at relatively low grazing angle, and the targets are ships at sea. In theory, this should not cause large difficulties, since receiver noise and reflections from targets should be the only components present at the output of the MTI filters. However, this is not necessarily the case when applied to magnetron radars. A set of MTI processed radar signals recorded from a typical ship radar are analysed. It shows that this particular signal exhibits different features than the theoretical assumptions, due to correlation between samples caused by the sea clutter. In addition, erroneous estimation of the transmitted frequency occurs for some pulses, which complicates the signal further. Thus, the input to the automatic detector is more than just receiver noise and targets. Other types of interference like land clutter, precipitation and other targets are not available for the analysis. However, based on the theoretical arguments presented in the previous chapter, the choice of CFAR detector is made in order to handle such situations as well. Thus, an OS CFAR detector is chosen as the first threshold, followed by a binary integrator. Analysis of the statistical properties of the signal after square-law detection is performed in order to predict the CFAR multiplier. Parameters for different distributions have been estimated, and expected theoretical performance is shown. The latter is for comparison to the results in the next chapter. Implementation, simulation and testing have been carried out using MATLAB and MATLAB Statistics Toolbox.

3.1 Material

As mentioned in the introduction to this chapter, a set of radar signals recorded from a shipborne radar are to be evaluated for the performance of the detector proposed in this thesis. Components in this signal will be presented here along with key parameters for the proceeding analysis. The recording radar was an X-band radar that uses a magnetron oscillator for amplification of transmitted pulses. Magnetron oscillators starts at a random phase for each pulse, and for this particular radar the transmitted frequency is 9410 ± 30 MHz. Signals has been recorded at IF frequency of 60 MHz, and the sampling frequency was $F_s = 40$ MHz. The recorded sector was $\pm 30°$ relative to the bow, and the range was approximately 1000 m. Each sector has been stored in one file, and the number of sectors used are 50. The pulses within each sector varies around 1100 and the number of samples in range are 258. Varying number of pulses per sector is caused by variation in the pulse repetition frequency (PRF). The starting phase of the oscillator is random, and needs to be measured or estimated if MTI processing is to be applied. There are several methods of doing this, but for this set of data, the transmitted frequency has been estimated from signal energy leaking through the duplexer [5, pp.182 – 184]. Occasionally, the phase estimator fails to estimate the starting phase. This occurs for 0 to 4 pulses in each sector, and results in pulses containing large clutter amplitudes for all range instances. Targets reflecting more than one pulse may be seen when the magnitude of the received pulses is displayed on a Plan Position Indicator (PPI) display, as shown in Figure 3.1.

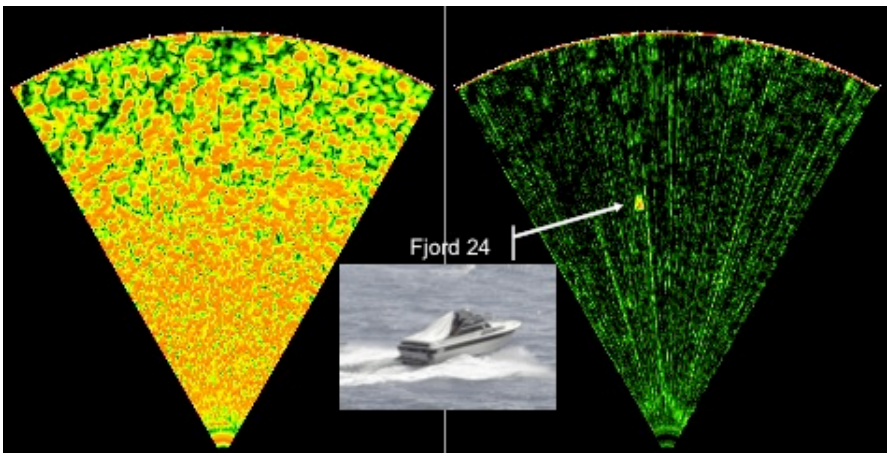

Figure 3.1: Magnitude of received pulses for one sector displayed on a PPI display. Left: Unprocessed radar signals. Right: MTI processed radar signals. The picture is taken from reference [1].

The width of the stop band in the MTI filters determines whether clutter components is passed through the filters or not. If slow moving targets are to be detected, the cut-off frequency needs be set at a fairly low Doppler frequency. As a consequence, some clutter components of high Doppler frequency may pass through the filters. This is only valid for moving clutter. The first samples in the range direction are components from the transmitted pulse that leak through the duplexer. The recorded signal contains reflection from sea clutter and a small pleasure craft. The pleasure craft represents the target in the proceeding analysis, and it is assumed to be a Swerling case 1 target. The antenna pattern is assumed to be Gaussian shaped within in the main lobe, and the number of pulses reflected by the target is given by,

$$n_b = \frac{60}{360}\frac{\text{PRF}}{\text{RPM}}\theta_{3\text{dB}}. \tag{3.1}$$

RPM is the Rounds Per Minute and $\theta_{3\text{dB}}$ is the beamwidth between the 3 dB points on each side of the main lobe. According to equation (A.2), the range resolution is $R_{\text{res}} = 22.5\text{m}$, and the number of samples herein is $\tau \cdot F_s = 6$.

Table 3.1: Radar parameters.

Transmitted frequency	9410 ± 30 MHz
IF	60 MHz
F_s	40 MHz
τ	150 ns
Polarization	Horizontal
$\theta_{3\text{dB}}$	1.23°
Mean PRF	2882 Hz
RPM	24.2
n_b	24
R_{res}	22.5m
# sectors	50
# pulses per sector	≈ 1100
# range samples	258
# samples in resolution cell	6

The radar parameters mentioned are summarized in Table 3.1. In Figure 3.2, 10 files have been superimposed after MTI processing and square-law detection to visualize the movement of the target. It can be observed that the number of pulses reflected by the target varies as the target moves in the environment. Also, the

pulses with erroneous phase estimation in the MTI processor are observed as lines in the range direction with large magnitudes. In the next section, the proposed automatic detector will be presented along with requirements to its performance.

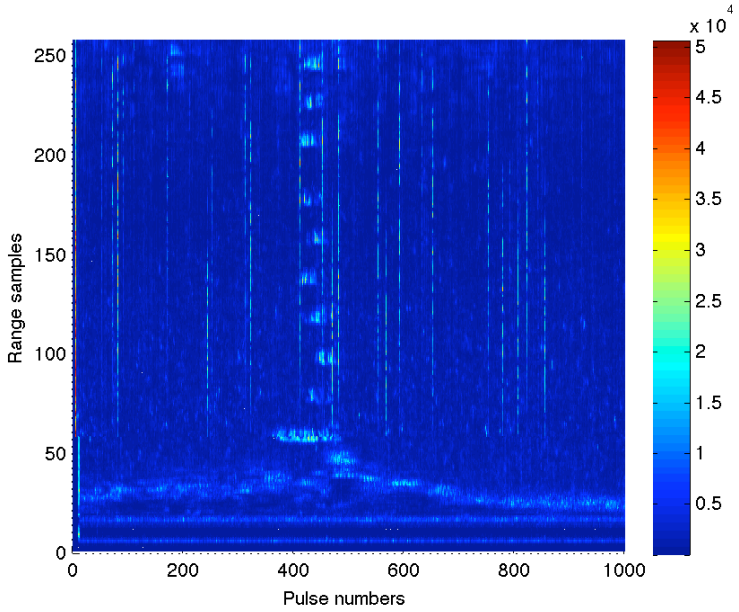

Figure 3.2: 10 sectors after MTI processing and square-law detection is superimposed in the same figure. The intensity is shown at the colorbar to the right. The target is the cluster of large magnitudes that move through the picture.

3.2 Automatic Detector

In this section, requirements to performance of the automatic detector is stated in order to provide guidelines for the design. As mentioned earlier, an OS CFAR with binary detection decision followed by a binary integrator is chosen for further investigation. A block diagram of the detector is shown in Figure 3.3. The detector is to be suited to and tested on the material presented in the previous section. The detector should minimize the false alarm probability, while detecting the targets in all of the recorded sectors. The CFAR multiplier is to be predicted from statistical analysis and compared to the true performance. In the next section, the signal will be examined in terms of correlation as it has an effect on the performance of the detector.

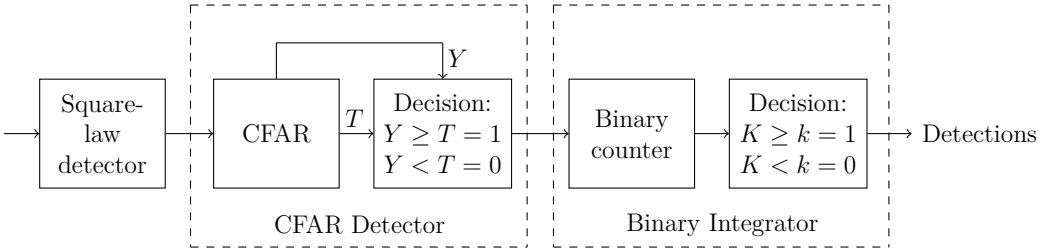

Figure 3.3: Block diagram of the automatic detector investigated in this thesis.

3.3 Correlation

Most of the theory on CFAR detection and binary integration is based on the assumption that the received signal samples are IID. Thus, the samples applied should be completely decorrelated in space and time. The question arise on whether the data described in Section 3.1 is correlated or not. This is an important point that needs to be investigated before analysis of the CFAR detector is to be carried out, and it is the topic of this section. In Section 2.2 and 2.6.4, the spatial correlation properties of sea clutter were discussed. It was assumed that the sea clutter consisted of Rayleigh distributed speckle and Gamma distributed mean level. This may be true when observing raw radar signals, but what happens after MTI processing? In theory, the correlation in range is determined by the transmitted pulse width. For the MTI processed signals, the spatial decorrelation length in terms of samples is $\tau \cdot F_s = 6$. This may also be seen by deriving the range autocorrelation function (ACF) [3, pp.37 – 39]. Assume one pulse with range samples from 0 to N after square-law detection. The ACF for the j'th lag is given as,

$$R_j = \sum_{i=1}^{N} (z_i - \bar{z})(z_{i+j} - \bar{z}), \tag{3.2}$$

where $\bar{z}$ is the estimated mean value. The normalized range correlation coefficient may be given as,

$$\rho_j = \frac{R_j}{R_0}, \qquad 0 \leq \rho_j \leq 1, \tag{3.3}$$

where R_0 is the variance of the square-law detected samples. The correlation coefficient is such that if $\rho_j = 1$, two samples are completey correlated. And if $\rho_j = 0$, two samples are completely uncorrelated. This shows the spatial correlation between the samples, and it is used to observe the behaviour of sea clutter in the light of the discussion in Section 2.2. The results differ from pulse to pulse due to the motion of

the sea clutter. ρ_j for one MTI processed radar pulse is shown in Figure 3.4. It may be observed that it exhibits some spikiness, which is caused by the spatial variation of the clutter component. Moreover, the correlation coefficients for several pulses may be averaged to indicate the overall decorrelation distance.

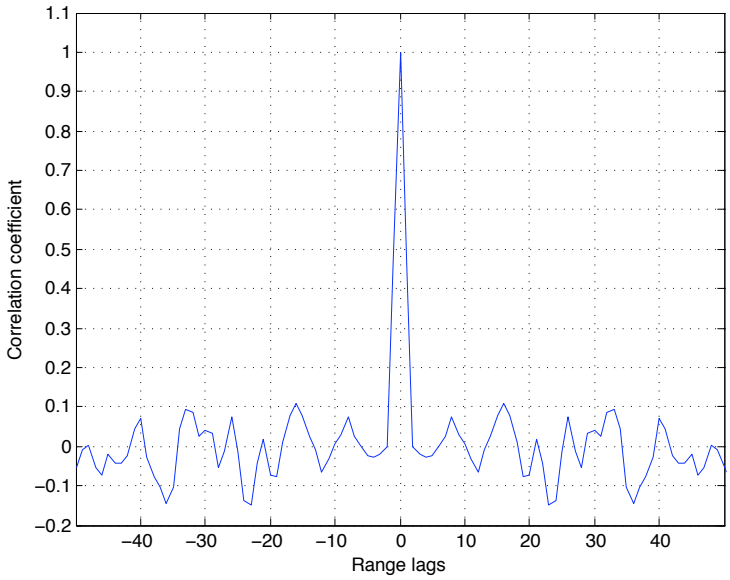

Figure 3.4: Range ACF of pulse one pulse after MTI processing and square-law detection.

This can be seen in Figure 3.5, where the correlation coefficient for 100 pulses containing clutter and noise have been averaged. It can be seen that the ρ is approximately equal to 0.1 at $j = 6$. Correlation in the azimuth direction is also of interest if all samples are to be used for analysis. The raw radar signals may be assumed to be correlated within the 3 dB beamwidth of the antenna, which is $n_b = 24$. After MTI processing, the pulses should be uncorrelated if the clutter component is completely removed. However, this is not the case, and it will be seen in the next chapter that false alarms occur when clutter components are detected in m out of n pulses. If independency between samples is required, decimation in range and azimuth might be necessary. By doing this, information will be lost from the received data which is unfortunate. Ideally, one should take the correlation into account and use all available samples when assessing data parameters and performance. But this is difficult for non-Gaussian variables [20]. Thus, if correlation properties are not to be included in the analysis, a compromise between performance and information loss must be considered. This is discussed in the next section, along with the choice of CFAR method. Also, parameters for the OS CFAR are decided.

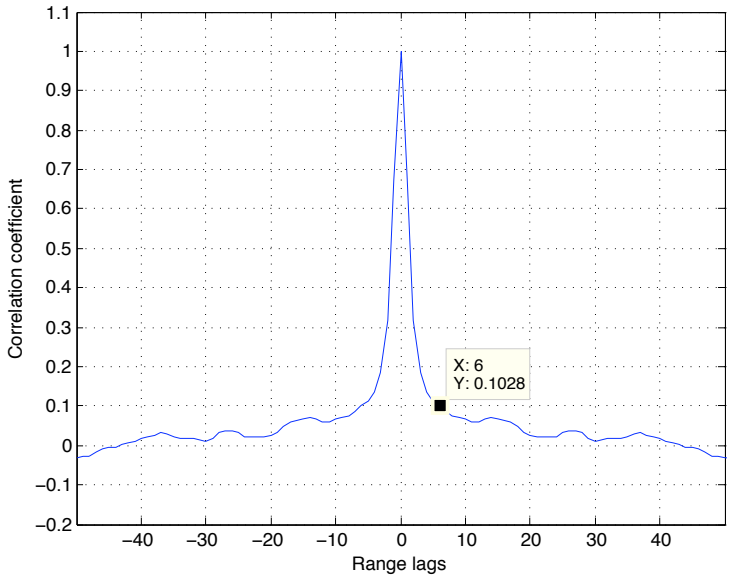

Figure 3.5: Range ACF averaged over 100 pulses after MTI processing and square-law detection. At $j = 6$ the correlation coefficient is approximately 0.1.

3.4 CFAR Method

The first thresholding will be performed by a CFAR processor. CFAR processors generate adaptive thresholds which increase the probability of detecting targets compared to fixed thresholds. As described in Chapter 2, the threshold is obtained by multiplying the estimated local clutter level with the CFAR multiplier α. Estimation of the local clutter level involves choosing a CFAR method and setting the parameters. From the discussion on CFAR methods, it was stated that CA CFAR is the CFAR method with highest detection probability in homogeneous backgrounds. However, it exhibits poor performance when a clutter edge or multiple targets are present. As the latter is often encountered in maritime environments, one may look towards other CFAR methods. The OS CFAR has worse performance in homogeneous environments than the CA CFAR, but is clearly superior in the presence of clutter edges and multiple targets. When considering MTI processed radar signals, one would assume that a great part of the clutter components would have been removed, and that clutter edges would not occur unless it moves with a Doppler velocity larger than the MTI threshold. Situations with multiple targets are more likely to be encountered, and it is desired to have a robust CFAR detector that is able to deal with such situations. Thus, the OS CFAR is chosen as the first thresholding for the detector even if it is at the expense of detection performance. When

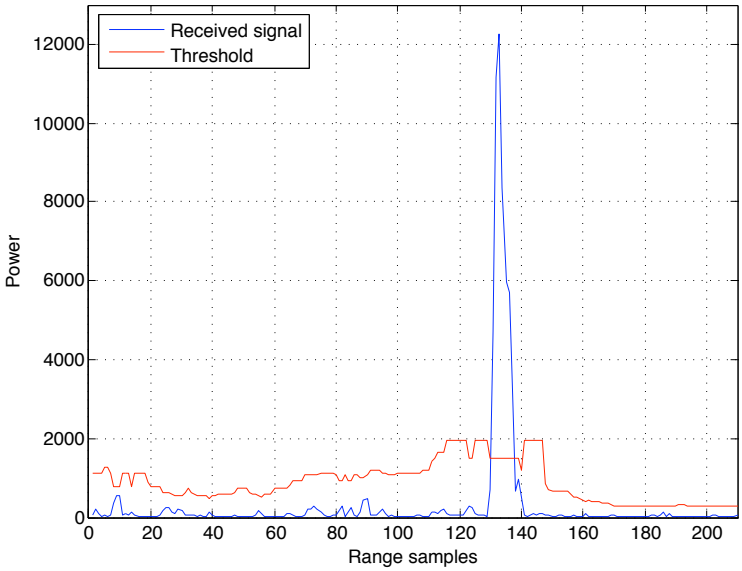

Figure 3.6: One pulse after MTI processing and square-law detection is plotted along with the threshold generated by the OS CFAR. The large peak crossing the threshold is reflections from the target. The CFAR parameters were $N = 48$ and $\alpha = 7.9$.

designing an OS CFAR detector, the number of reference cells N and the ordered statistic k need to be chosen. One reference cell is equal to the size of one range resolution cell. The number of samples per range resolution cell is 6, and the number of range resolution cells available is 43. If this regime is to be implemented, it will be difficult to obtain enough thresholds for the environment in the recorded data as N is usually chosen to be between 8 and 32 [10]. In addition, as discussed in the previous section, decimation of the samples will result in loss of information. Thus, it is decided to keep all samples, and N will be denoted as the number of reference samples instead of reference cells in the proceeding analysis. In Section 2.5.2, it was stated that k should be chosen such that $k = (3/4)N$. Moreover, $N - k$ should not be less than twice the extension of the target if multiple targets are to be detected. When observing Figure 3.6, it can be seen that the target has an extension of approximately 8-12 samples. Thus, twice the target length corresponds to $16 \leq N - k \leq 24$ and $64 \leq N \leq 96$ samples. However, since only one target is present in the recorded data, N will be set to 36, 40 and 48 which corresponds to $N - k = 8, 10, 12$. It should be emphasized that if the detector is to be applied in a practical radar system, N should be increased to detect multiple targets. The threshold generated by the OS CFAR is also shown in Figure 3.6. A binary

threshold decision is applied after generation of the threshold. This is done in order to directly apply a binary integrator as the next step in the detection process. In the next section, analysis of the statistics of the clutter environment and fitting of distributions will be carried out in order to derive the CFAR multiplier.

3.5 Statistical Analysis

The estimate of the local clutter level derived by the OS CFAR detector is to be multiplied with a CFAR multiplier which is derived from the clutter statistics. What family of distributions that may fit sea clutter has been discussed widely in literature. The most common distributions used is the Exponential, Weibull, Log-Normal and K-distribution. Thus, the question is which family of distributions does the MTI processed signals fit? This will be investigated in this section. It should be emphasized that the objective is not to find the distribution that may fit sea clutter in general, but what distribution fits the clutter plus noise components at the output of the MTI filter. Receiver noise is assumed to be Rayleigh distributed, and square-law detection of this yields Exponential distributed data. However, clutter components is also present in the MTI processed data. This may indicate that longer tailed distributions may be better models than the Exponential distribution. Nevertheless, it should not be left out of analysis. In addition to finding the family of distributions that may fit the signal, parameters for the distributions need to be estimated. This will be shown next.

3.5.1 Estimating Parameters

A common approach to finding the parameters for distributions is the Maximum Likelihood Estimation, as described in Section 2.7. MLE finds the parameters that are closest to the empirical distribution of a fixed data set, and it is applicable to all distributions. Expressions for the MLE of parameters for Log-Normal, Weibull and K-distribution are shown in reference [20]. With the use of fit functions in MATLAB Statistics Toolbox, the parameters for Exponential, Weibull and Log-Normal distribution are derived. For K-distribution, the parameters are solved numerically. The results are shown in Table 3.2. It should also be noted that the parameter estimation has been carried out after square-law detection. The MLE method assumes IID samples. Since all samples in the data set are applied to the MLE method, correlation is present and estimates may be incorrect. On the other hand, if the estimated parameters provide fairly good fits one may assume that the method serves its purpose. It is possible that other parameter estimation methods

Table 3.2: Estimated parameters for the distributions.

Exponential		Log-Normal		Weibull		K-distribution	
$\hat{\bar{z}}$	129.57	$\hat{\mu}$	3.70	$\hat{B}$	91.53	$\hat{b}$	0.01
-	-	$\hat{s}$	1.68	$\hat{C}$	0.6445	$\hat{v}$	1.20

would yield better results. But this will not be investigated in this thesis. Next, the goodness of fit for each distribution is evaluated.

3.5.2 Fitting Distributions

The MLE parameters derived in the previous section may yield the best fitted distribution for each family. But are the obtained distributions good models of the data? To answer this question, probability plots may be utilized as a visual assessment for the goodness of fit. The idea is to alter the y-axis in a graph so that the theoretical CDF will fall on a straight line. By plotting the theoretical CDF along with the empirical data points, it is possible to observe whether the data belongs to the theoretical model or not. If the empirical data is near the straight line, one may conclude that the assumed model is a good approximation to the data. By using probability plots, different statistical models may be compared to empirical results without complicated mathematics. It has the advantage of emphasizing the tails in the distributions, which are important if low P_{fa} is to be obtained. Since low P_{fa} is desired in most CFAR detectors, attention should be directed to the region $0 \leq P_{fa} \leq 10^{-3}$ when analyzing the plots. The probability plots for Exponential, Log-Normal and Weibull distributions are derived using probability plot functions in MATLAB. The results are shown in Figure 3.7. It is evident that none of the suggested distributions fit the data without errors. The Exponential distribution fits the data quite well for small values but departs from the reference line for values larger than approximately 170. At these points, larger values are observed than what is expected for a Exponential distribution. This may be interpreted as a heavier tail in the empirical PDF, which is in agreement with what was suspected earlier. As a consequence, large errors in P_{fa} and P_d will be observed if the fitted Exponential distribution is to be used for calculation of α. Comparison with the fitted Log-Normal distribution shows departure from the reference line in several regions. At the crossing, points the empirical distribution matches the theoretical distribution, and may provide correct estimates of α. However, the region of interest does not contain more than two crossing points, which limits the freedom in choosing correct values. The fitted Weibull distribution does not seem to fit the data in the

high valued region either. For comparison with the K-distribution, the empirical CDF has been plotted on a logarithmic scale along with the fitted distribution in Figure 3.8. The upper plot may indicate that the K-distribution is a good fit for the data. However, closer inspection of the tails indicates that some error should be expected for this distribution as well. As a quantitative measure, the mean square error (MSE) between the empirical CDF and the different distributions has been derived. The MSE for N samples is calculated by,

$$\text{MSE} = \frac{1}{N}\sum_{i=1}^{N}(P(z_i) - \tilde{P}(z_i))^2, \tag{3.4}$$

where $P(z_i) = P(Z \leq z_i)$ for the theoretical CDF, and $\tilde{P}(z_i) = \tilde{P}(Z \leq z_i)$ for the empirical CDF. The results is shown in Table 3.3, and it may be concluded that the K-distribution is the best fitted distribution.

Table 3.3: Mean Square Error between the theoretical and empirical CDFs.

Distribution	Exponential	Log-Normal	Weibull	K
MSE	$1.81 \cdot 10^{-2}$	$5.28 \cdot 10^{-4}$	$4.41 \cdot 10^{-4}$	$2.69 \cdot 10^{-4}$

In the proceeding analysis, the Exponential distribution will be left out of the analysis. This is due to the poor goodness of fit, and it is expected that this model will only exhibit large errors for the P_{fa} values of interest. In the next section theoretical P_{fa} is derived for the distributions in order to give guidelines for the choice of CFAR multiplier.

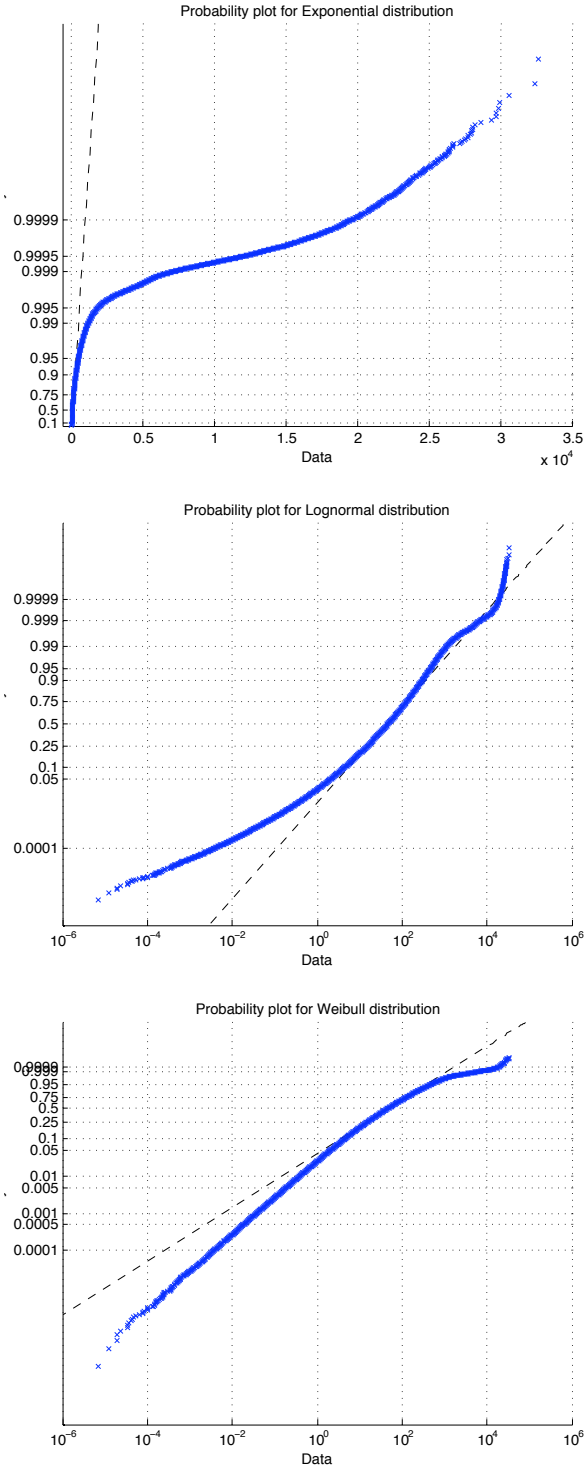

Figure 3.7: Probability plots for Exponential, Weibull and Log-Normal distribution. The observed sample points is square-law detected.

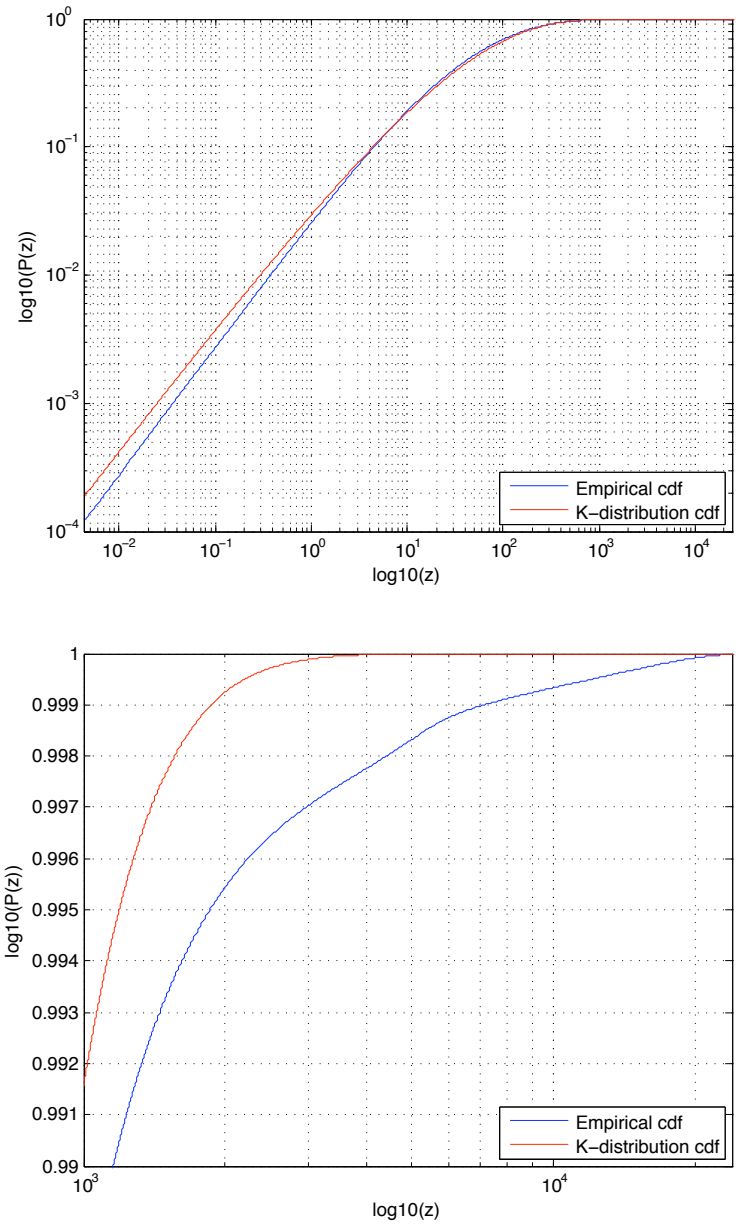

Figure 3.8: In the upper figure, the theoretical and empirical CDF for K-distribution are plotted after square-law detection. In the lower figure, the tail of the distributions are emphasized.

3.6 CFAR Multiplier

The analysis in the previous section was on fitting distributions to the clutter plus noise component in the MTI processed radar signal. This was to find suitable models for predicting the CFAR multiplier α. The next step in the process is to derive α for a given CFAR method, and the theoretical results will be shown in this section. Expression for this was given by equation (2.12), and solving for Exponential and Weibull distributions yield equation (2.18) and (2.21). For Log-Normal and K-distribution, no analytic expressions were found, and numerical integration needs to be applied. The common approach when designing a CFAR detector is to require a fixed value for P_{fa}, and calculate α. This is achieved by changing α iteratively until the desired P_{fa} is obtained. Results of these efforts are shown for Log-Normal, Weibull and K-distribution in Figure 3.9, 3.10 and 3.11. The range of P_{fa} was $0 \leq P_{fa} \leq 10^{-6}$, and the parameters employed is the MLE parameters in Section 3.5.1. In accordance with Section 3.4, the CFAR parameters are set to $N = 32, 40, 48$ and $k = (3/4)N$. When comparing the plots it is observed that larger CFAR multipliers are required for the Log-Normal distribution than the other distributions. With large CFAR multipliers it may be understood that the CFAR detector is configured to a long tailed clutter or noise distribution. As the Log-Normal distribution is the model with the longest tail, this seems reasonable.

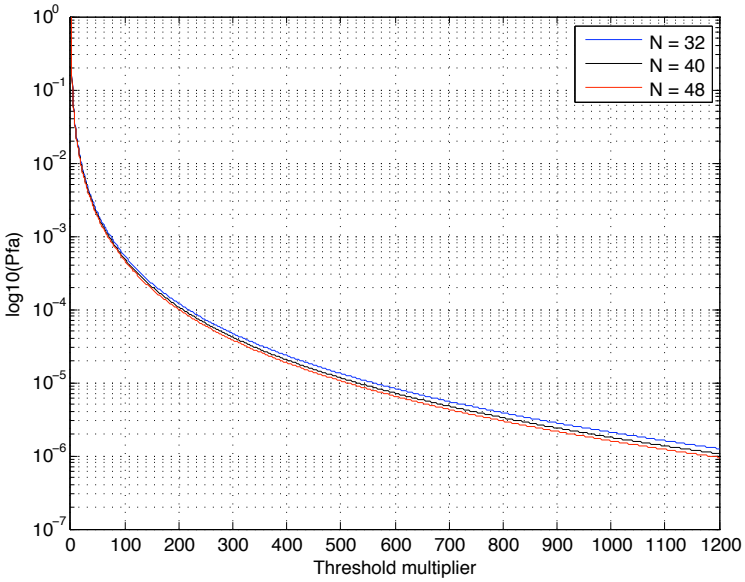

Figure 3.9: P_{fa} versus α for OS CFAR with Log-Normal distributed clutter after square-law detection. $k = (3/4)N$ and the parameters are $\hat{\mu} = 3.7$ and $\hat{s} = 1.68$.

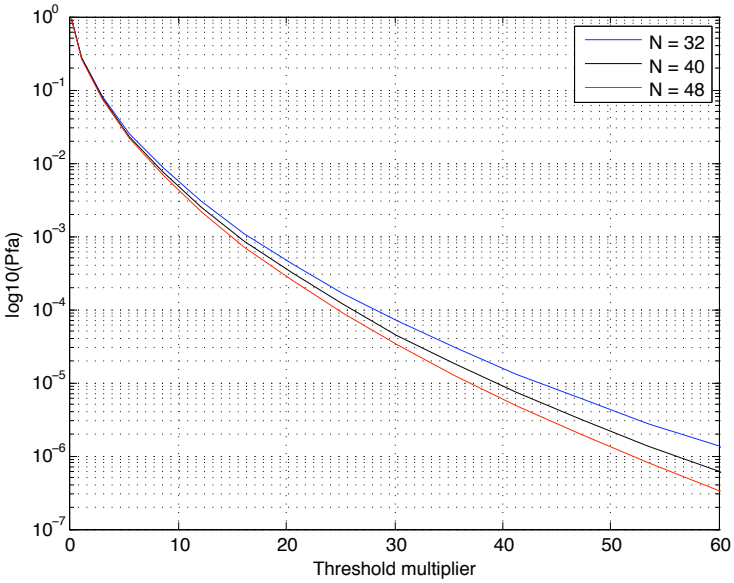

Figure 3.10: P_{fa} versus α for OS CFAR with Weibull distributed clutter after square-law detection. The parameters are $\hat{B} = 91.53$ and $\hat{C} = 0.6445$.

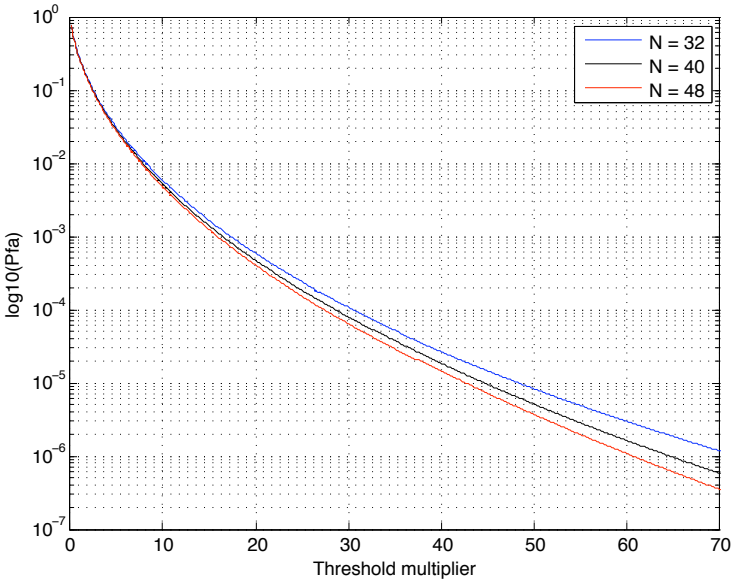

Figure 3.11: P_{fa} versus α for OS CFAR with K-distributed clutter after square-law detection. The parameters are $\hat{b} = 0.01$ and $\hat{v} = 1.2$.

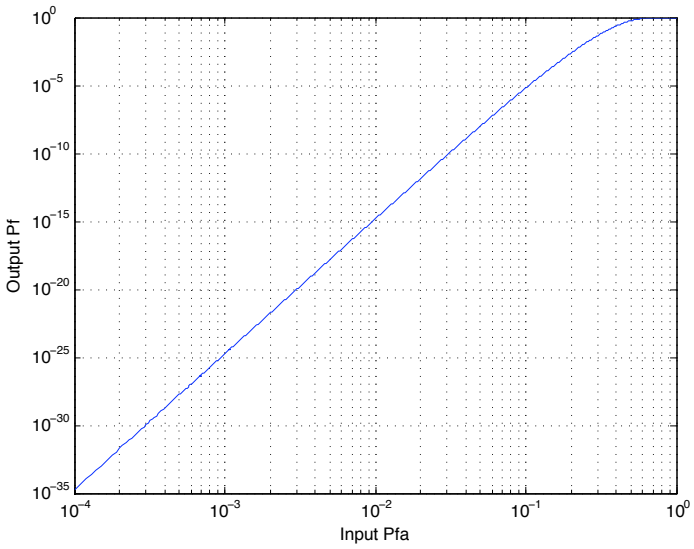

Figure 3.12: Output P_f as a function of input single pulse P_{fa}. The parameters are $n = 20$ and $m = 10$.

The Weibull and K-distribution yield lower values of α than the Log-Normal distribution. They may yield better prediction of α, as the MSE values shown in the previous section were smaller. These results will be used for comparison when measuring the performance when the MTI processed data is applied. In the next section, the design of the binary integrator will be presented.

3.7 Binary Integrator

The next step in the automatic detector is the binary integrator. The binary integrator is also termed as binary detector, double-threshold detector or m-out-of-n detector [5, p.292]. Utilization of this second threshold is motivated by its ability to reduce the number of false alarms. This can be crucial for the purpose of the detector as the CFAR detection may exhibit poor performance due to correlation and inaccurate modelling of the clutter. Design of the binary integrator will be shown in this section, and expected theoretical performance will be given for comparison to the results in Chapter 4. As shown in Figure 3.3, the binary integrator is applied after the OS CFAR. The output of the OS CFAR is binary such that 1's and 0's denotes detections and non-detections respectively, and the binary integrator may be applied directly. Parameters were given in Section 2.8, and it was stated that n should be chosen to be $n = 0.84n_b$. Thus, $n \approx 20$ according to the value of n_b given

in Table 3.1. Also, m was given as $m_{opt} \approx 10^b n^a$. The target in the MTI processed radar signals may be considered as a Swerling case 1 target, thus $m_{opt} \approx 10$. With these parameters the output P_f is shown as a function of the input single pulse P_{fa} in Figure 3.12. This will be used for comparison with the results in the next chapter. In order to illustrate the binary output, detections of one target is shown in Figure 3.13. The figure has been generated by mapping each detection in several pulses to the corresponding range and pulse instances. Thus, each red circle corresponds to a 1 at the output of the binary integrator. As seen by the figure, the target produces several detections. The number of detections is dependent on the detector configuration and the target SCR. In addition, the input signal is shown above, where reflections from the target are presented as the area with larger intensity than the surroundings. It should be mentioned that the two plots are of the same target, but on different scales. In the next chapter, the results from testing of the automatic detector will be presented and discussed.

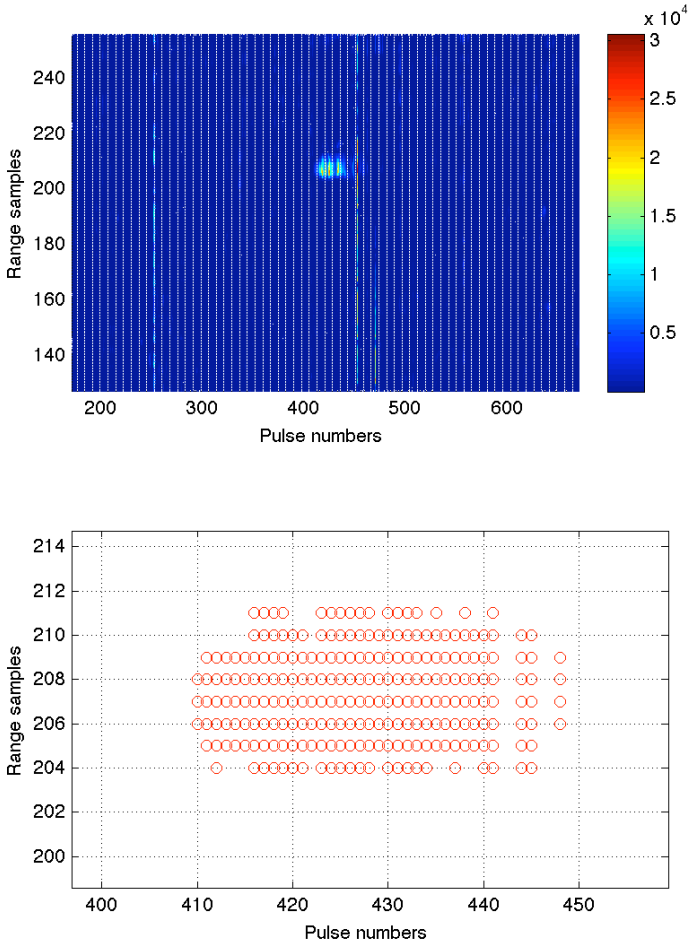

Figure 3.13: The upper figure shows a number of consecutive input pulses to the detector with one target incorporated. The color bar to the right represent the intensity, and the target is in the area of larger intensity than the surroundings. The lower figure shows the resulting output of the detector. The parameters were $N = 48$, $k = (3/4)N$, $\alpha = 7.9$, $n = 20$ and $m = 10$.

Chapter 4

Results and Discussion

In the previous chapter, requirements for the for the automatic detector were established, and it was designed in accordance to theory and evaluation of the recorded MTI processed radar data. The expected theoretical performance was presented for various configurations of the OS CFAR detector, and expected false alarm probability at the output of the binary integrator was shown as a function of P_{fa}. This gives guidelines for what quantities that may be of interest when testing the detector, and the results will be presented in this chapter. Measured parameters will be denoted with a tilde. The probability of false alarm and the probability of detection is, in a strict sense, measurements that requires infinitely large data sets if true values is to be obtained. Obviously, such measurements is not possible in practice. However, if the data set is large, measured values may be close to the truth. Unfortunately, this is not the case when values of $\tilde{P}_{fa} < 10^{-4}$ is to be measured for the available MTI radar data. The measured values are merely estimates of P_{fa}, and it is derived as the percentage of detections in a set of samples containing clutter plus noise. This set is constructed by picking a number of pulses from the 50 sectors where no reflections from the target is present. The pulses chosen are shown in Figure 4.1. Regarding P_d, the total energy that is actually received from target reflections is quiet difficult to identify in the recorded samples. Thus, when evaluating the detection performance it will rather be on the number of sectors containing any reflection from the target. This will at least give the opportunity for comparison between different configurations of the detector, as it is desired to detect the target in as many sectors as possible. The MTI radar data does not possess ideal properties in a probabilistic sense. In particular, correlation between samples will ensure deviation from the expected theoretical performance. The impact of this, and configurations required to obtain the best performance for the recorded data is shown.

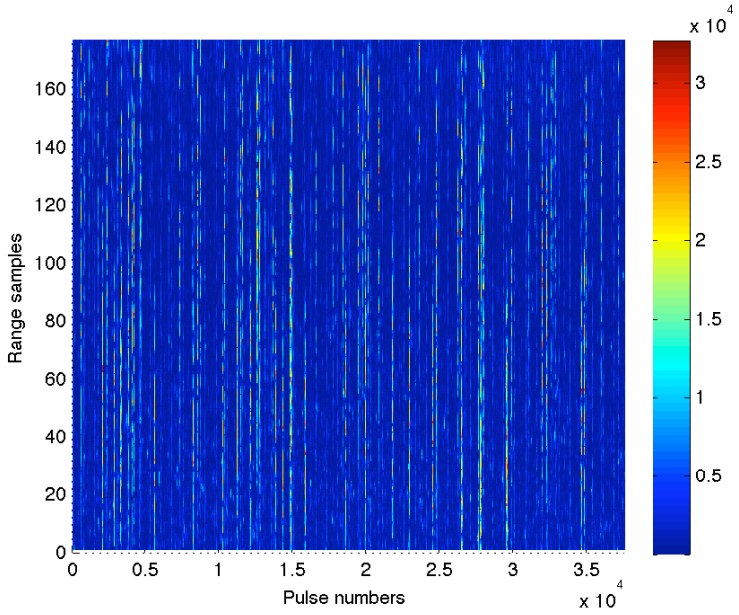

Figure 4.1: Plot of the dataset containing clutter plus noise components after square-law detection. The color bar to the right represents the intensity.

4.1 Probability of False Alarm

According to Section 3.2, the false alarm probability should be as small as possible while detecting the target in all sectors. Values of P_{fa}, α and P_f were derived in the previous chapter, and in this section, the measured $\tilde{P}_{fa}$ will be compared to the theoretical performance. Also, the measured $\tilde{P}_f$ as a function of input $\tilde{P}_{fa}$ will be shown for the binary integrator. Measurements of the false alarm probabilities are derived by dividing the number of sample detections with the total number of samples in a dataset containing clutter and noise only. Values of α are chosen from the plots in Section 3.6 such that $P_{fa} = 10^{-2}, 10^{-3}$ and 10^{-4}. Results when using the Log-Normal distribution is shown in Table 4.1. It is observed that the values for $\tilde{P}_{fa}$ are smaller than the theoretical values. This deviation may be expected as the Log-Normal distribution is the distribution with the longest tail. As mentioned in the introduction to this chapter, the values for $\tilde{P}_{fa} < 10^{-4}$ may not be representative as the number of samples is limited. Nevertheless, one may conclude that prediction of CFAR multipliers using Log-Normal distribution yields too large thresholds. In Table 4.2 the results when using Weibull distribution are shown. For $P_{fa} = 10^{-2}$ the CFAR multiplier seems too high, and for $P_{fa} = 10^{-3}$ and $P_{fa} = 10^{-4}$ it seems slightly low. However, these results are closer to the theoretical values than the values measured for Log-Normal distribution.

Table 4.1: Measured $\tilde{P}_{fa}$ for Log-Normal CFAR multiplier.

	$N = 32$		$N = 40$		$N = 48$	
P_{fa}	α	$\tilde{P}_{fa}$	α	$\tilde{P}_{fa}$	α	$\tilde{P}_{fa}$
10^{-2}	19.6	$7.94 \cdot 10^{-4}$	18.9	$9.98 \cdot 10^{-4}$	18.4	$1.10 \cdot 10^{-3}$
10^{-3}	73.4	$2.07 \cdot 10^{-5}$	70.2	$3.19 \cdot 10^{-5}$	68.1	$4.09 \cdot 10^{-5}$
10^{-4}	217.6	$3.09 \cdot 10^{-7}$	207.0	$9.76 \cdot 10^{-7}$	200.1	$1.37 \cdot 10^{-6}$

Table 4.2: Measured $\tilde{P}_{fa}$ for Weibull CFAR multiplier.

	$N = 32$		$N = 40$		$N = 48$	
P_{fa}	α	$\tilde{P}_{fa}$	α	$\tilde{P}_{fa}$	α	$\tilde{P}_{fa}$
10^{-2}	8.1	$5.20 \cdot 10^{-3}$	7.7	$6.10 \cdot 10^{-3}$	7.5	$6.50 \cdot 10^{-3}$
10^{-3}	16.5	$1.20 \cdot 10^{-3}$	15.5	$1.50 \cdot 10^{-3}$	14.9	$1.70 \cdot 10^{-3}$
10^{-4}	28.2	$3.32 \cdot 10^{-4}$	26.0	$4.82 \cdot 10^{-4}$	24.6	$6.12 \cdot 10^{-4}$

Table 4.3: Measured $\tilde{P}_{fa}$ for K-distribution CFAR multiplier.

	$N = 32$		$N = 40$		$N = 48$	
P_{fa}	α	$\tilde{P}_{fa}$	α	$\tilde{P}_{fa}$	α	$\tilde{P}_{fa}$
10^{-2}	8.2	$5.10 \cdot 10^{-3}$	7.8	$5.90 \cdot 10^{-3}$	7.6	$6.40 \cdot 10^{-3}$
10^{-3}	17.3	$1.10 \cdot 10^{-3}$	16.5	$1.30 \cdot 10^{-3}$	15.9	$1.50 \cdot 10^{-3}$
10^{-4}	30.5	$2.72 \cdot 10^{-4}$	28.6	$3.86 \cdot 10^{-4}$	27.4	$4.80 \cdot 10^{-4}$

The same trend is seen for the K-distribution in Table 4.3. It may be seen that values of $\tilde{P}_{fa}$ is slightly closer to the theoretical than the Weibull distribution for $P_{fa} = 10^{-3}$ and 10^{-4}. Considering the mathematical complexity involved in using K-distribution, the use of Weibull distribution might seem more tractable. Extensive computation has been carried out to obtain $\tilde{P}_{fa}$ for a broad range of α for the MTI processed radar signals, and the results is shown in Figure 4.2. The graph shows that smaller N yields smaller $\tilde{P}_{fa}$. This is in disagreement with the graphs presented in Section 3.6, where theory states that smaller N should yield larger P_{fa}. This may be explained by the fact that theory gives performance for IID samples. In other words, the graphs in Section 3.6 can be understood as CFAR performance in Log-Normal, Weibull or K-distributed noise. On the other hand, the partially correlated clutter

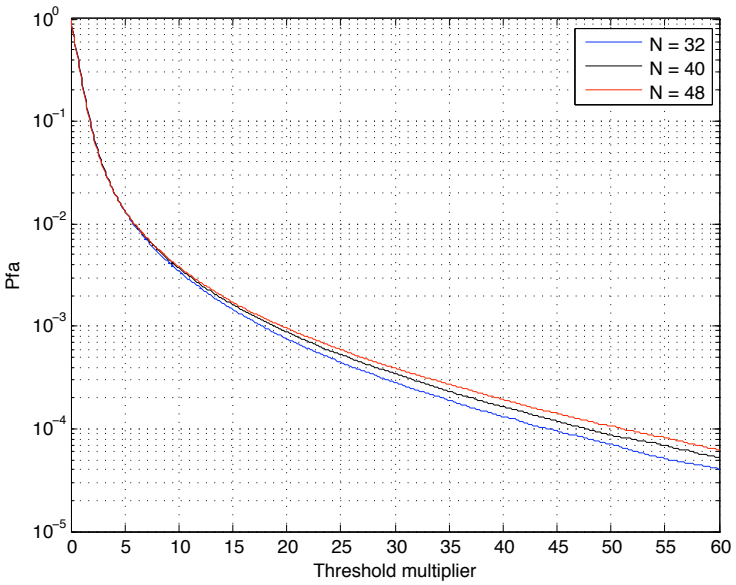

Figure 4.2: $\tilde{P}_{fa}$ at the output of the OS CFAR as a function of α.

actually appears as targets. That is, some wave at sea reflecting Doppler frequencies within the passband of the MTI filter may reflect n_b correlated pulses. Recall that n_b pulses was the number of pulses within the 3 dB beamwidth of the antenna given by equation (3.1). In reference [9], it is shown that increasing N results in increased P_d for OS CFAR. This may explain the results in Figure 4.2, since the clutter appears as targets with small SNR. Increasing N will obviously increase the number of detections on each target, and produce larger $\tilde{P}_{fa}$. For convenience, the detector has been tested on a synthetic Weibull distributed set of data. The applied parameters were equal to $\hat{B}$ and $\hat{C}$ derived in Section 3.5.1, and the result is shown in Figure 4.3. This is in accordance with the expected response when changing N. Also, comparing this to Figure 3.10, it can be seen that the response is almost equal. In Figure 4.4, the measured false alarm probability for the binary integrator, $\tilde{P}_f$, is plotted as a function of $\tilde{P}_{fa}$. The performance is worse than the theoretical performance shown in Figure 3.12. This may also be explained by the correlation between the samples in azimuth for the target like reflections of clutter. If the false alarm samples exceeds m within n samples, the binary integrator will not remove any of them, and $\tilde{P}_f$ will be increased. In the next section, the detections of the target will be measured in order to find maximum values of α before the detector fails to detect the target.

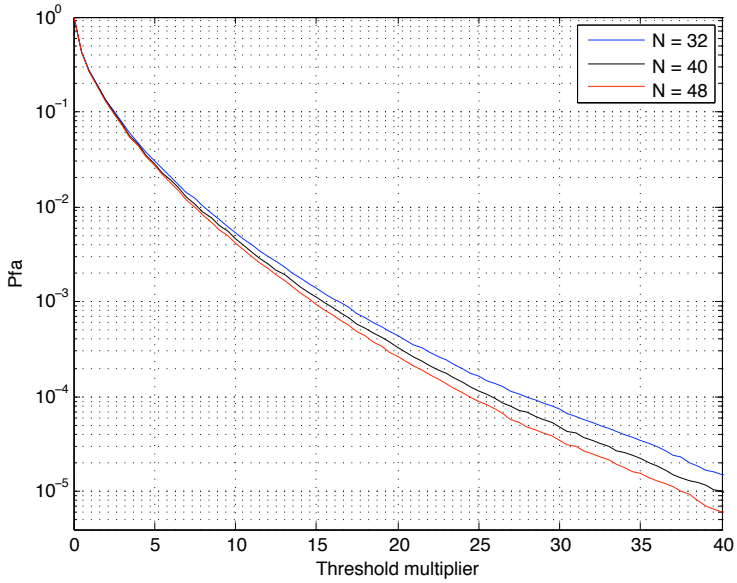

Figure 4.3: $\tilde{P}_{fa}$ as a function of α for a synthetic Weibull distributed data sets. The parameters are $\hat{B} = 91.53$ and $\hat{C} = 0.6445$.

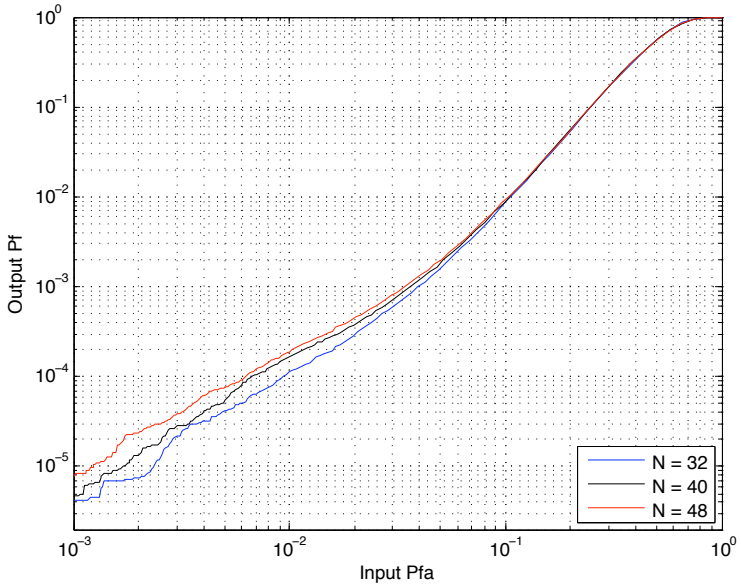

Figure 4.4: $\tilde{P}_f$ as a function of $\tilde{P}_{fa}$ for the binary integrator.

4.2 Target Detection

In order to set an upper limit for the CFAR multiplier, detections of the target may be measured. In terms of probability of detection P_d, all samples containing signal energy reflected by the target should be used. This number is difficult to obtain with a recorded signal since the energy reflected by the target may spread over numerous surrounding samples down to clutter level. In addition, energy reflected from noise and clutter is incorporated in the reflections from the target due to scattering and multipath propagation. Because of this, P_d will not be measured. However, it is possible to observe whether any detections occur in the region where the target is located or not. Thus, a target area is defined for each of the 50 sectors. Any detection within the target area will lead to the conclusion of target presence in the sector. This will be termed as a sector detection. Counting the number of sector detections may give some measure of the detection performance. This is carried out on the output of the binary detector only. The reason for not doing this at the output of the OS CFAR is that for the $\tilde{P}_f$ of interest, $\tilde{P}_{fa}$ is fairly large. Thus, false alarms may occur in the target region, and lead to increased $\tilde{P}_d$. This can be seen by comparing the two plots in Figure 4.9, where the detections at the output of the OS CFAR and the binary integrator is shown separatly.

Table 4.4: Sector detections are measured for various configurations of the automatic detector. The corresponding $\tilde{P}_{fa}$ and α are also shown.

$N = 32$			
$\tilde{P}_f$	$\tilde{P}_{fa}$	α	# sector detections / sectors
10^{-3}	$3.93 \cdot 10^{-2}$	2.9	50/50
10^{-4}	$9.41 \cdot 10^{-3}$	6	47/50
10^{-5}	$2.37 \cdot 10^{-3}$	12	17/50
$N = 40$			
$\tilde{P}_f$	$\tilde{P}_{fa}$	α	# sector detections / sectors
10^{-3}	$3.61 \cdot 10^{-2}$	3	50/50
10^{-4}	$6.73 \cdot 10^{-3}$	7.3	47/50
10^{-5}	$1.70 \cdot 10^{-3}$	14.7	33/50
$N = 48$			
$\tilde{P}_f$	$\tilde{P}_{fa}$	α	# sector detections / sectors
10^{-3}	$3.33 \cdot 10^{-2}$	3.1	50/50
10^{-4}	$6.37 \cdot 10^{-3}$	7.6	50/50
10^{-5}	$1.25 \cdot 10^{-3}$	17.6	40/50

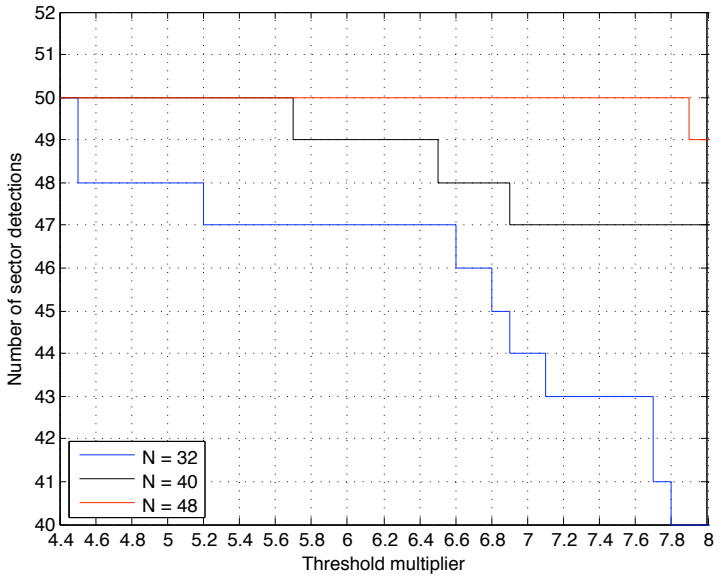

Figure 4.5: The number of sector detections are counted for a range of α values for each value of N at the output of the binary integrator. The total number of sectors are 50.

In addition, the output of the binary integrator is of overall interest, and will be the focus in the further analysis. The results for fixed values of $\tilde{P}_f$ are shown in Table 4.4. It can be seen that for $\tilde{P}_f = 10^{-3}$, all the choices of N yield target detections in all sectors. For the other values of $\tilde{P}_f$, the number of sector detections is increased when increasing N. This might be expected from the discussion on false alarms caused by sea clutter in the previous section, since increasing N results in increased $\tilde{P}_d$. In particular, it can be seen that $N = 48$ is the only configuration that is able to detect the target in all sectors and maintain $\tilde{P}_f = 10^{-4}$. It can also be deduced that the target will be detected in all sectors for values of α smaller than those corresponding to $\tilde{P}_f = 10^{-3}$. In order to find some maximum value of α before the detector fails to detect targets, the sector detections were measured for some range of α values. The critical region is shown in Figure 4.5. It can be seen that the maximum values before detection failure is $\alpha = 4.5$ for $N = 32$, $\alpha = 5.7$ for $N = 40$ and $\alpha = 7.9$ for $N = 48$. Thus, for $N = 48$ a broader range of α values can be chosen without loss of sector detections. The corresponding $\tilde{P}_{fa}$ and $\tilde{P}_f$ is shown in Table 4.5. The table shows that the lowest false alarm probability is $\tilde{P}_f = 8.96 \cdot 10^{-5}$. In Figure 4.6, the detections in 10 sectors have been superimposed in the same plot. This is shown in order to get a visual impression of the detections of the moving target. Reflections from the target are marked with red color, and false alarms is

Table 4.5: False alarm probabilities at maximum values of α.

N	α	$\tilde{P}_{fa}$	$\tilde{P}_f$
32	4.5	$1.65 \cdot 10^{-2}$	$2.18 \cdot 10^{-4}$
40	5.7	$1.07 \cdot 10^{-2}$	$1.79 \cdot 10^{-4}$
48	7.9	$6.00 \cdot 10^{-3}$	$8.96 \cdot 10^{-5}$

marked with blue color. For clarity, it should be mentioned that the colored areas are a number of small circles, similarly to Figure 3.13. Also, the input pulses before detection are shown for comparison. In Figure 4.7, the detections are shown for the configurations in Table 4.4 when $N = 48$. For $\tilde{P}_f = 10^{-3}$, numerous false alarms are observed at close range. This is caused by leakage of the transmitted pulses through the duplexer, and reflections from the bow of boat carrying the radar. Also, it can be seen that no false alarms occur in the 10 sectors when $\tilde{P}_f = 10^{-5}$, but the target is only detected in 8 of the sectors. The detections for the maximum values of α is shown in Figure 4.8. It can be seen that $N = 48$ and $\alpha = 7.9$ yields the smallest number of false alarm clusters in the 10 sectors. This is in accordance with Figure 4.2, when comparing to the other values of α shown. When observing the plots of the detections, it can be noticed that the false alarms appears in clusters. Again, this may be explained by the correlation between samples in the range and azimuth direction for the sea clutter. If a false alarm occurs in one sample after CFAR detection, it is likely that false alarms also occur in neighboring samples. If the detections extend over more than m out of n pulses in the azimuth direction, the binary integrator will fail to reject the false alarms. However, stand alone false alarms will be removed effectively, as seen in Figure 4.9. In the next chapter, conclusions from the observations in this chapter and Chapter 3 will be drawn.

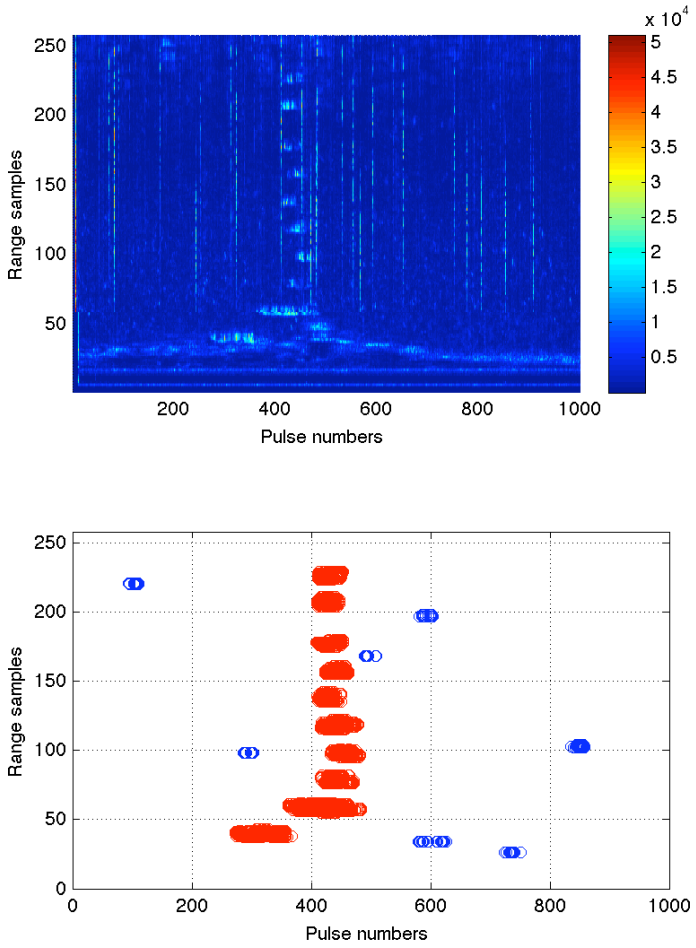

Figure 4.6: The upper figure shows 10 sectors of the MTI processed radar signal superimposed in the same plot after square-law detection. The colorbar to the right represents the intensity. The lower figure shows detections at the output of the automatic detector on the same signal. The parameters were $N = 48$, $\alpha = 7.9$, $m = 10$, and $n = 20$.

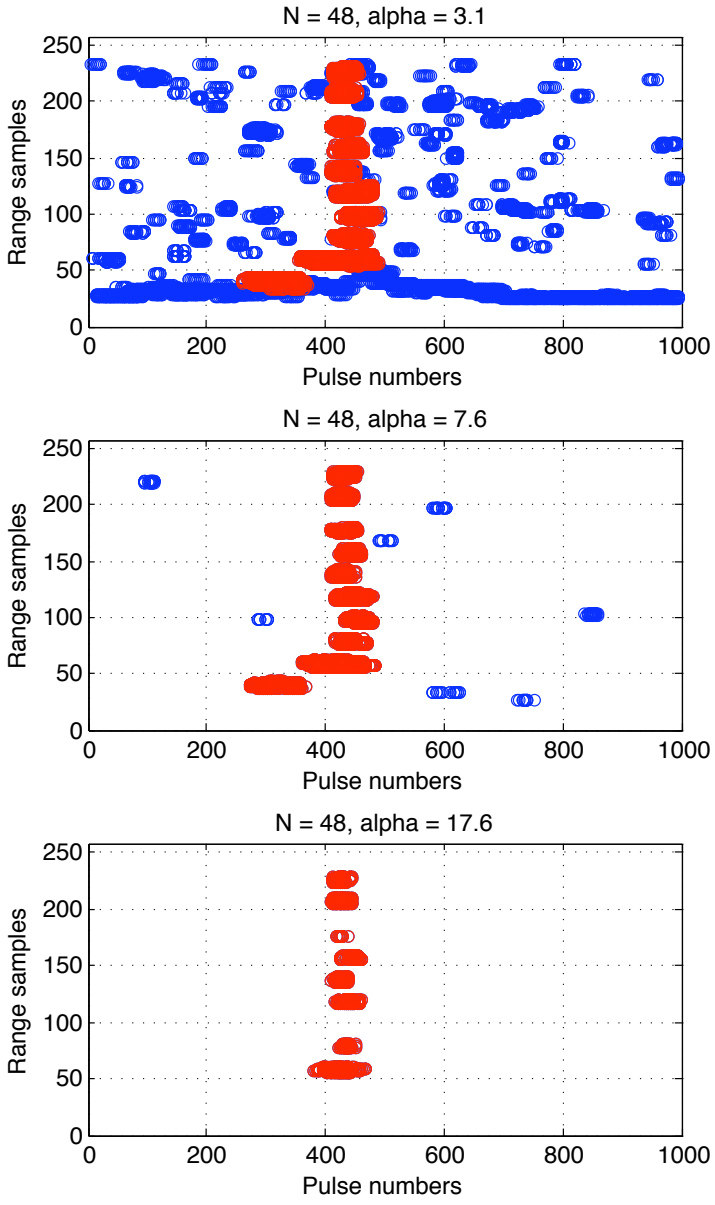

Figure 4.7: Detections at the output of the automatic detector in 10 sectors are superimposed in the figures. Values of α are set according to Table 4.4 and $N = 48$. Thus, the false alarm rates are $\tilde{P}_f = 10^{-3}, 10^{-4}$ and 10^{-5} for the upper, middle and lower figure, respectively. The parameters of the binary integrators were $m = 10$ and $n = 20$.

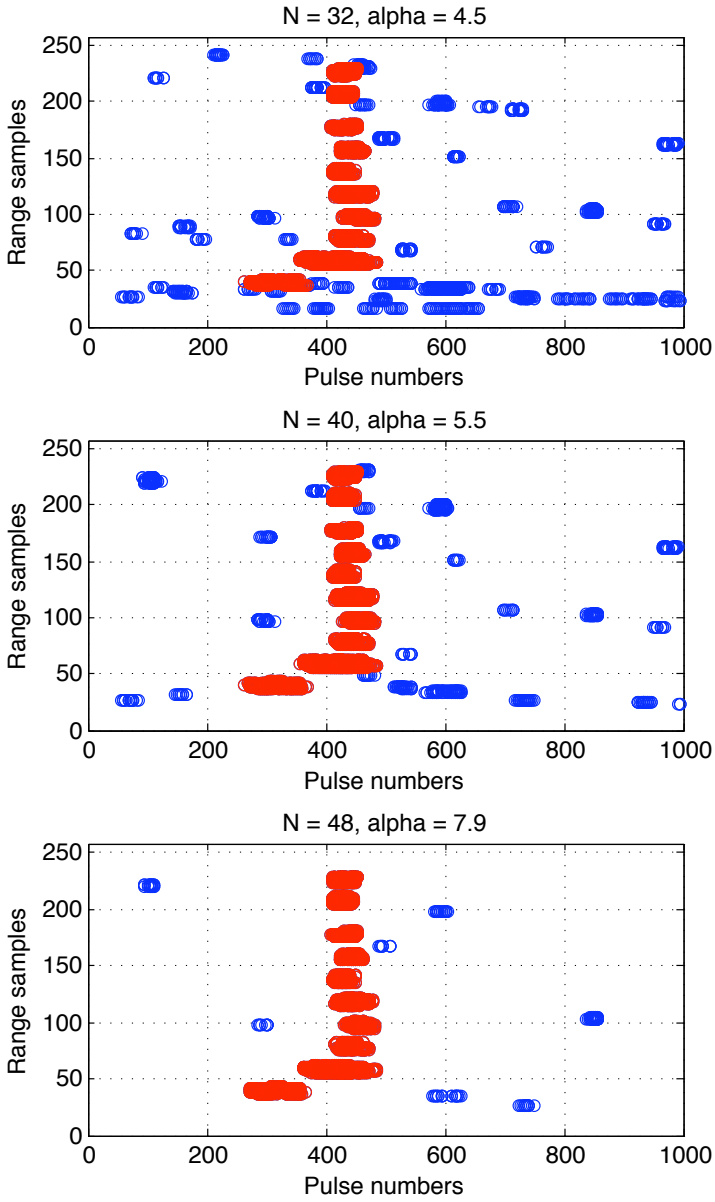

Figure 4.8: Detections at the output of the automatic detector in 10 sectors are superimposed in the same figures. The values of α are set according to the maximum values in Figure 4.5 before the detector fails to detect the target in certain sectors. The parameters of the binary integrators were $m = 10$ and $n = 20$.

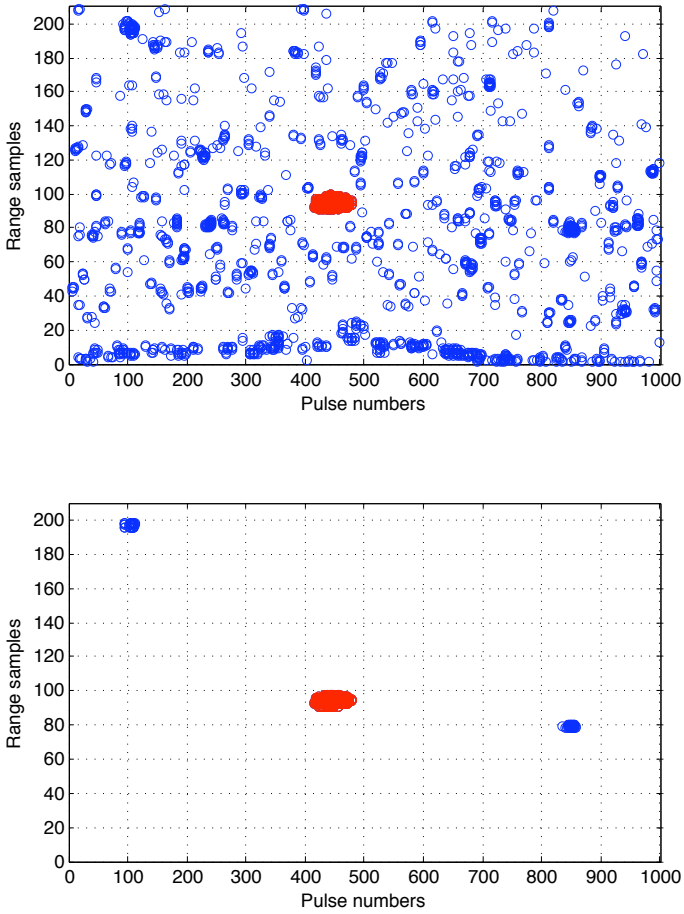

Figure 4.9: The upper figure shows detections at the CFAR output for one sector, and the lower figure shows detections at the output of the binary integrator. The parameters were $N = 48$, $\alpha = 7.6$, $m = 10$ and $n = 20$.

Chapter 5

Conclusion

In this chapter, conclusions will be drawn based on the observations and discussions made in the previous chapters. The OS CFAR was chosen as the first threshold because of its performance in non-homogeneous environments. The number of reference samples N was set such that $N-k$ was in the vicinity of the targets extension in range, and $k = (3/4)N$. For the second threshold, a binary integrator was chosen. This was motivated by its significant performance in reducing the false alarm rate, and the simple mathematics involved. Its parameters were solely based on assumptions made from theory.

From the analysis of the MTI processed data, it has been shown that the samples exhibit spatial correlation. This was explained by the sea clutter components that is passed through the MTI filter, which affects the detector performance. In particular, the measured $\tilde{P}_{fa}$ for the OS CFAR was shown to be larger when increasing the number of reference samples N. This was in disagreement with theory, where an increase in N results in an decrease in $\tilde{P}_{fa}$. However, clutter components may appear as targets, as it is correlated in the range and azimuth direction. This explained the result, since an increase in N results in an increase of detection probability of targets.

In order to derive the CFAR multiplier, different distributions has been fitted to the MTI data using MLE. It was shown that K-distribution provided the best fit for $\tilde{P}_{fa} = 10^{-3}$ and 10^{-4}. While for $\tilde{P}_{fa} = 10^{-2}$ the Weibull distribution was closer. Due to the small differences in $\tilde{P}_{fa}$ between the two distributions, it was suggested that using the Weibull distribution may be more tractable as it involves simpler mathematics. $\tilde{P}_{fa}$ was also measured using a Log-Normal distribution. As this distribution yielded too large CFAR multipliers, it was concluded that the Log-Normal distribution is not a suitable model for the MTI processed data. For the binary integrator, the measured false alarm rate $\tilde{P}_f$ was shown to be worse than the

theoretical P_f. This was explained by the correlation between clutter samples in the azimuth direction.

The false alarm rate may be decreased infinitely, but in order to detect targets, upper limits for the CFAR multipliers must be found. Thus, the detectors ability to detect targets was investigated. As the probability of detection is difficult to obtain from recorded data, the approach was on sector detections rather than sample detections. If the target is to be detected in all of the recorded sectors, the maximum CFAR multipliers was found to be $\alpha = 4.5, 5.7$ and 7.9 for $N = 32, 40$ and 48, respectively. It was shown that increasing N results in increased number of sector detections. This also increases the measured $\tilde{P}_f$ for a fixed α. However, for fixed values of $\tilde{P}_f$, the number of sector detections was increased when increasing N. Thus, among the parameters tested, it may be concluded that $N = 48$ and $\alpha = 7.9$ yield a minimum false alarm probability of $\tilde{P}_f = 8.96 \cdot 10^{-5}$ while detecting the target in all sectors.

The automatic detector designed in this thesis may be used in practical applications for detecting targets in MTI processed signals. However, the detector was not tested in the presence of multiple targets, and the values of N was limited. Also, the measured performance was restricted by the number of samples available. In the next chapter, proposals to further work on these matters is presented along with suggestions to additional functions for the automatic detector.

Chapter 6

Further work

In this chapter, suggestions to further work on the automatic detector is presented. As mentioned previously, the number of reference samples N was restricted to values such that $N - k$ was in the vicinity of the range extension of the target. According to [10], this distance should be doubled in order to detect two targets without masking. The performance of the OS CFAR for multiple targets is investigated in [9], but various values of N should also be investigated for the detector when it is combined with a binary integrator. In addition, larger data sets should be tested in order to get more accurate estimates for false alarm rates below 10^{-4}.

Other types of clutter, such as land or rain, was not available for analysis in this thesis. If the automatic detector is to be implemented in practical applications, this should be investigated. Also, the performance should be tested in the presence of clutter edges and multiple targets.

Spatial correlation between samples was discovered in the MTI signal, and it was shown that it has an impact on the expected performance. The author believes that for practical purposes, it is not advantageous to carry out decimation even if it provides IID samples. Less accuracy in calculation of the thresholds, and loss of information may worsen the performance. If the MTI filter can be optimized such that no clutter components is present in the passband of the filter, the correlation will be reduced and may improve the detector performance.

Other and more sophisticated CFAR methods, such as the Trimmed Mean CFAR and Censored Ordered Statistics CFAR may perform better than the detector proposed in this thesis. Such detectors may be tested to the MTI signal, but the mathematical complexity will probably increase when the CFAR multiplier is to be calculated for distributions like the K-distribution. Nevertheless, computer techniques like numerical integration may be applicable in order to overcome the obstacles.

If it is desired to extract the targets position and movement, tracking may be applied after automatic detection. Tracking typically involves clustering of detections, and calculation of the most probable target position from scan to scan. Methods on tracking filters and handling of position measurement errors may be reviewed in reference [24].

Bibliography

[1] E. Løvli and Y. Steinheim, *MTI for magnetronradar. En populærvitenskapelig introduksjon*, June 2009.

[2] M. Ihlen, *Non-coherent pulse integration and automatic detection of MTI processed radar signals*. Norwegian University of Science and Technology, Desember 2010.

[3] K. Ward, R. Tough, and S. Watts, *Sea Clutter: Scattering, K Distribution and Radar Performance*. The Institution of Engineering and Technology, 2006.

[4] S. Watts, "Radar Detection Prediction in Sea Clutter using the Compound K-distribution Model," *Proc,IEE,Part F*, vol. 132, November 1985.

[5] M. Skolnik, *Introduction to Radar Systems*. New York: McGraw-Hill, 3rd ed., 2001.

[6] M. Bassem, *Radar System Analysis and Design using Matlab*. Chapman and Hall/CRC, 2000.

[7] M. Skolnik, *Radar Handbook*. McGraw-Hill, 3rd ed., 2008.

[8] F. Nathanson, *Radar Design Principles - Signal Processing and the Environment*. SciTech Publishing, 2nd ed., 1999.

[9] P. Gandhi and S. Kassam, "Analysis of CFAR Processors in a Nonhomogeneous Background," *IEEE Transactions on Aerospace and Electronic systems*, vol. 24, July 1988.

[10] H. Rohling, "Radar CFAR Thresholding in Clutter and Multiple Target Situations," *IEEE Transactions on Aerospace and Electronic systems*, vol. AES-19, July 1983.

[11] N. Levanov and M. Shor, "Performances of Order Statistics CFAR," *IEEE Transactions on Aerospace and Electronic systems*, vol. 27, March 1991.

[12] R. Walpole, R. Myers, S. Myers, and Y. Keying, *Probability and Statistics for Engineers and Scientists*. Pearson Education, Inc., 8th ed., 2007.

[13] N. Levanov and M. Shor, "Order statistics CFAR for Weibull background," *Proc,IEE,Part F*, vol. 137, June 1990.

[14] P. Weber and S. Haykin, "Ordered Statistic Processing for Two-Parameter Distributions with Variable Skewness," *IEEE Transactions on Aerospace and Electronic systems*, vol. AES-21, November 1985.

[15] V. Anastassopoulos and G. Lampropoulos, "Optimal CFAR Detection in Weibull Clutter," *IEEE Transactions on Aerospace and Electronic systems*, vol. 31, January 1995.

[16] E. Al-Hussaini, "Performance of an Ordered Statistic CFAR Processor in Log-Normal Clutter," *Electronics Letters*, vol. 24, March 1988.

[17] E. Jakeman and P. Pusey, "A Model for Non-Rayleigh Sea Echo," *IEEE Transaction on Antennas and Propagation*, November 1976.

[18] K. Ward, C. Baker, and S. Watts, "Maritime Surveillance Radar," *Proc, IEE, Part F*, vol. 137, April 1990.

[19] B. Armstrong and H. Griffiths, "CFAR Detection of Fluctuating Targets in Spatially Correlated K-distributed Clutter," *Proc, IEE, Part F*, vol. 138, April 1991.

[20] I. Antipov, *Analysis of Sea Clutter Data*. Salisbury, South Australia: DSTO Electronic and Surveillance Research Laboratory, 1998.

[21] M. Richards, *Fundamentals of Radar Signal Processing*. New York: McGraw-Hill, 2005.

[22] D. Shnidman, "Binary Integration for Swerling Target Fluctuations," *IEEE Transactions on Aerospace and Electronic systems*, vol. 34, July 1998.

[23] L. Blake, "The Effective Number of Pulses Per Beamwidth for a Scanning Radar," *Proceedings of the IRE.*, vol. 41, June 1953.

[24] M. Stakkeland, *Tracking in Radar Surveillance Systems*. PhD thesis, Norwegian University of Science and Technology, January 2010.

[25] P. Swerling, "Probability of Detection for Fluctuating Targets," *IRE Transactions*, vol. 6, April 1960.

[26] H. David and N. H.N., *Order Statistics*. John Wiley and Sons Inc, 3rd ed., 2003.

[27] N. McLachlan, *Bessel functions for Engineers*. London: Oxford University Press, 1st ed., 1934.

[28] J. Tunaley, *K-distribution Algorithm*. London Research and Development Corporation, August 2010.

[29] H. Meikle, *Modern Radar Systems*. Artech House, 2nd ed., 2008.

Appendix A

The Resolution Cell

The resolution cell is the radars ability to seperate two targets in the spatial domain, and it is determined by the radars configuration. This principle will be presented in this appendix and it is convenient to start with the radar equation. The radar equation gives the power received by a receiving antenna. If the transmitting and receiving antenna is the same antenna, the equation for the two-way propagation is given as,

$$P_r = \frac{P_t G A_e \sigma}{(4\pi)^2 R^4} = \frac{P_t G^2 \lambda^2 \sigma}{(4\pi)^3 R^4}, \tag{A.1}$$

where $A_e = G\lambda^2/4\pi$. The other factors are given as:

P_t = Power transmitted

G = Antenna gain

A_e = Effective area of receiving antenna

λ = Wavelength

σ = Backscatter cross section

R = Distance from antenna to target

Additional loss factors also applies for the expression above, but they are not necessary for this analysis and are omitted. The resolution cell is the radars ability to

resolve targets in the range and azimuth direction. The resolution in range is given by,

$$R_{\text{res}} = \left(\frac{c\tau}{2}\right) \sec \phi, \tag{A.2}$$

where τ is the pulse width, c is the speed of light and ϕ is the grazing angle. At small grazing angles $\sec(\phi) \approx 1$ and may be omitted. The azimuth resolution is,

$$A_{\text{res}} = 2R \tan(\theta_B/2), \tag{A.3}$$

where R is range and θ_B is the beamwidth. For small beamwidths, $\tan(\theta_B/2) \approx \theta_B/2$. Multiplying the two equations yield the area of the resolution cell. That is,

$$A = \left(\frac{c\tau}{2}\right) R\theta_B \sec \phi. \tag{A.4}$$

The principle is shown in Figure A.1. From the resolution cell the radar equation for surface clutter may be derived. The backscatter cross section for an area containing a number of independent individual scatterers is given by $\sigma = A\sigma^0$, where σ^0 is the backscatter coefficient. The latter is calculated as the clutter cross section per unit area. Substituting equation (A.4) into (A.1) gives the reflected power from surface clutter. Thus,

$$P_c = \frac{cP_tG^2\lambda^2\tau\theta_B\sigma^0}{2^7(\pi R)^3}, \tag{A.5}$$

assuming small grazing anle and small beamwidth. The theory in section is taken from [21, ch.1] [5, ch.7].

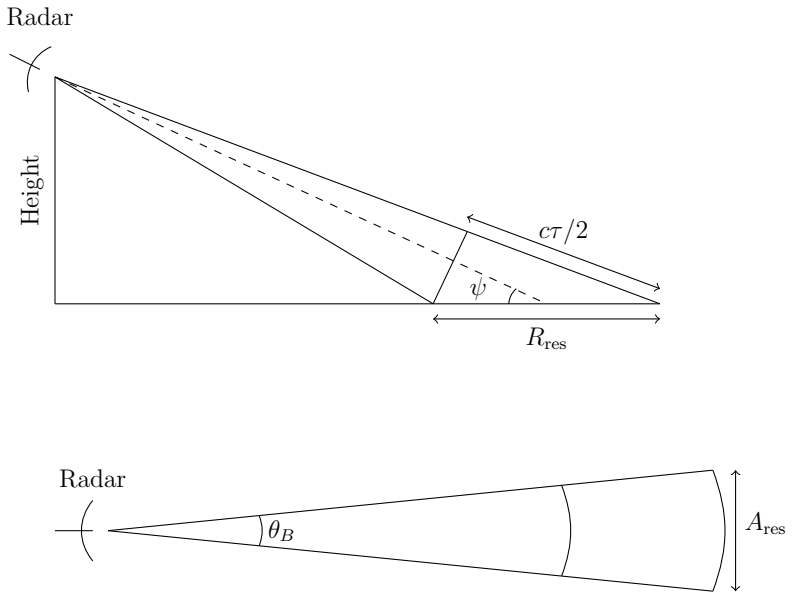

Figure A.1: The upper figure illustrates the range resolution cell, where ψ is the grazing angle. The lower figure illustrates the azimuth resolution cell, where θ_B is the azimuth beamwidth.

Appendix B

The Doppler Effect

When the radar illuminates a moving target, the received frequency will different from what was transmitted. This is called the Doppler effect and is used in MTI radar processing, and a brief introduction to the concept will be given in this appendix. For the two-way propagating radar, the phase change in the received signal may be written as

$$\phi = 2\pi \frac{2R}{\lambda_c} = 4\pi R/\lambda \tag{B.1}$$

where λ_c is the wavelength of the transmitted signal at carrier frequency f_c, and R is the range to the target. Differentiating this with respect to time gives the rate of change for the phase. That is

$$\omega_d = \frac{d\phi}{dt} = \frac{4\pi}{\lambda_c}\frac{dR}{dt} = \frac{4\pi v_r}{\lambda_c} = 2\pi f_d \tag{B.2}$$

where v_r is the radial velocity, and f_d is the doppler frequency shift. Thus, f_d may be written as

$$f_d = \frac{2v_r}{\lambda_c} \tag{B.3}$$

The received frequency is dependent on the direction of the moving target. Approaching targets yield a positive change in the received frequency, and receding targets yield a negative change. Thus, the received frequency may be written as $f' = f_c \pm f_d$, where $f' = c/\lambda'$. Also, if the angle θ between the targets velocity vector and the radars line of sight is different from 0° or 180°, the radial velocity

may be written as $v_r = v\cos(\theta)$, where v is the true target speed. The concept is illustrated in Figure B.1, and it is utilized in radars employing MTI and Pulse Doppler processing, as discussed in Section 2.3. The theory derived here is taken from [5, ch.3.1] [6, ch.1.4].

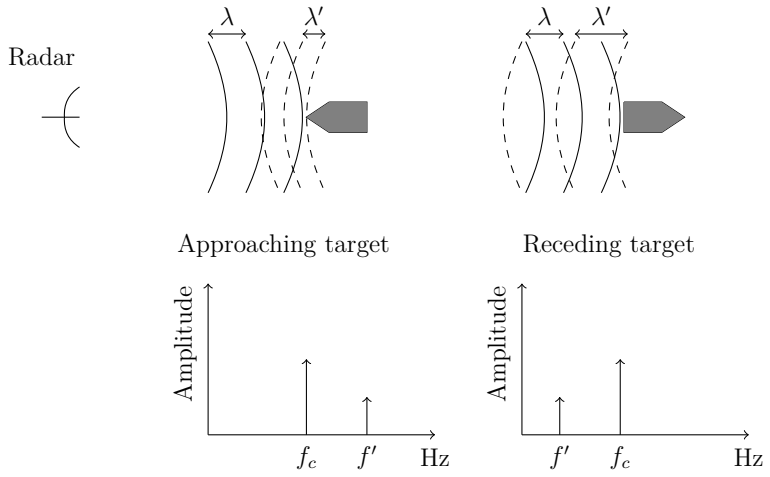

Figure B.1: Illustration of the Doppler effect: The solid lines represent the transmitted wave, and the dashed lines are the reflected wave. If the target is approaching the radar, the reflected wavelength λ' is smaller than the transmitted wavelength λ. This causes a positive Doppler shift of the transmitted frequency, thus $f' > f_c$. If the target is receding, the effect is opposite.

Appendix C

Swerling Target Models

The Swerling target models were proposed by Peter Swerling in 1954, and used to describe the received pulses from fluctuating targets [25]. The models are widely used in literature, and will be repeated in this appendix.

- **Case 1** The power of the received pulses from a target is assumed to be constant during a single scan, but to fluctuate independently from scan to scan. The fluctuations of the target cross section σ are assumed to follow the Exponential distribution. That is,

$$p(\sigma) = \frac{1}{\bar{\sigma}} \exp\left(-\frac{\sigma}{\bar{\sigma}}\right), \tag{C.1}$$

  where $\sigma \geq 0$ and $\bar{\sigma}$ is the average value of target cross section [5, p.66].

- **Case 2** The PDF of the target cross section is the same as for case 1, but the fluctuations are now independent from pulse to pulse.

- **Case 3** The radar cross section is assumed to be constant within a single scan and independent from scan to scan. And the PDF of the radar cross section is given by,

$$p(\sigma) = \frac{4\sigma}{\bar{\sigma}^2} \exp\left(-\frac{2\sigma}{\bar{\sigma}}\right). \tag{C.2}$$

- **Case 4** The PDF of the target cross section is the same as for Case 2, but the fluctuations are now from pulse to pulse.

- **Case 0** The target cross section is nonfluctuating from pulse to pulse and scan to scan.

Appendix D

Order Statistics

In this appendix, the CDF of the OS CFAR power estimate $X_{(k)}$ will be given according to [26], and the derivation of the PDF will be shown. Assume a set of variables $X_1, ..., X_N$ with CDF $F_X(x)$. The probability of an order statistic variable $X_{(k)}$ being less than or equal to some value x is given by the sum of Bernoulli trials with the number of successes j increasing from k to N. This yields,

$$F_{X_{(k)}}(x) = P(X_{(k)} < x) = \sum_{j=k}^{N} \binom{N}{j} F_X(x)^j (1 - F_X(x))^{N-j}. \tag{D.1}$$

The PDF is obtained by differentiating $F_{X_{(k)}}(x)$ with respect to x. Thus,

$$\begin{aligned} f_{X_k}(x) &= \frac{d}{dx} F_{X_{(k)}}(x) \\ &= \sum_{j=k}^{N} \binom{N}{j} \Big[j F_X(x)^{j-1} (1 - F_X(x))^{N-j} \\ &- (N-j) F_X(x)^j (1 - F_X(x))^{N-j-1} \Big] f_X(x) \\ &= N \sum_{j=k}^{N} \left[\binom{N-1}{j-1} F_X(x)^{j-1} (1 - F_X(x))^{N-j} \right. \\ &- \left. \left(\binom{N}{j} - \binom{N-1}{j-1} \right) F_X(x)^j (1 - F_X(x))^{N-j-1} \right] f_X(x) \end{aligned}$$

$$
\begin{aligned}
f_{X_k}(x) &= N\left[\binom{N-1}{j-1}F_X(x)^{k-1}(1-F_X(x))^{N-k}\right. \\
&\quad \left. - \binom{N-1}{N}F_X(x)(1-F_X(x))^{-1}\right] f_X(x) \\
&= N\binom{N-1}{j-1}F_X(x)^{k-1}(1-F_X(x))^{N-k}f_X(x) \\
&= k\frac{N!}{(k-1)!(N-k)!}F_X(x)^{k-1}(1-F_X(x))^{N-k}f_X(x) \\
&= k\binom{N}{k}F_X(x)^{k-1}(1-F_X(x))^{N-k}f_X(x). \qquad \text{(D.2)}
\end{aligned}
$$

This expression is used in Section 2.6 for derivation of P_{fa} and the CFAR multiplier α.

Appendix E

K-Distribution

In this appendix, the derivation of the K-distribution statistics will be shown. The K-distribution is a compound distribution based on the discussion in Section 2.2. The two components are a Rayleigh distributed scatterer and a Gamma distributed mean level. The PDF of the Rayleigh scatterer may be written in terms of its dependence on the mean power $\bar{z}$, such that,

$$p(x|\bar{z}) = \frac{2x}{\bar{z}} e^{\left(-\frac{x^2}{\bar{z}}\right)}, \qquad 0 \leq x \leq \infty. \tag{E.1}$$

The varying mean level is a random variable itself, and its PDF may be written as,

$$p(\bar{z}) = \frac{b^v}{\Gamma(v)} \bar{z}^{\,v-1} e^{(-b\bar{z})}, \qquad 0 \leq \bar{z} \leq \infty, \tag{E.2}$$

where b is the scale parameter and v is the shape parameter. The PDF of the compound distribution is given as,

$$p(x) = \int_0^\infty p(x|\bar{z}) p(\bar{z})\, d\bar{z} = \frac{2b^v x}{\Gamma(v)} \int_0^\infty \bar{z}^{\,v-1} \exp\left(-b\bar{z} - x^2/\bar{z}\right) d\bar{z}. \tag{E.3}$$

To solve this integral, the modified besselfunction of second kind may be used. Equation (126) in [27, p.165] gives the following relation,

$$K_v(u) = \int_0^\infty e^{-u\cosh(\theta)} \cosh(v\theta)\, d\theta, \qquad R(u) > 0. \tag{E.4}$$

By substituting $\bar{z} = xe^\theta/\sqrt{b}$ in equation (E.3), the derivation of the PDF may be carried out as follows:

$$
\begin{aligned}
p(x) &= \frac{2b^v x}{\Gamma(v)} \int_0^\infty \left[\frac{xe^\theta}{\sqrt{b}}\right]^{v-2} \exp\left(-\sqrt{b}x(e^\theta + e^{-\theta})\right) \left[\frac{xe^\theta}{\sqrt{b}}\right] d\theta \\
&= \frac{2b^v x}{\Gamma(v)} \left[\frac{x}{\sqrt{b}}\right]^{v-1} \int_0^\infty e^{\theta(v-1)} \exp\left(-2\sqrt{b}x\cosh(\theta)\right) d\theta \\
&= \frac{4b^{\frac{v+1}{2}} x^v}{\Gamma(v)} \int_0^\infty \cosh(\theta(v-1)) \exp\left(-2\sqrt{b}x\cosh(\theta)\right) d\theta \\
&= \frac{4b^{\frac{v+1}{2}} x^v}{\Gamma(v)} K_{v-1}(2\sqrt{b}x).
\end{aligned}
$$

The CDF may be calculated in the same manner, as the probability of a threshold crossing is determined by a Rayleigh distributed variable modulated with a Gamma distributed mean level. The probability of a Rayleigh distributed variable crossing a threshold x_T is,

$$
P(x > x_T|\bar{z}) = \int_{x_T}^\infty p(x|\bar{z})\, dx = \exp(-x_T^2/\bar{z}). \tag{E.5}
$$

Inserting this in (E.3), the probability of exceeding the x_T for a K-distributed variable is,

$$
P(x > x_T) = \int_0^\infty \exp(-x_T^2/\bar{z}) p(\bar{z})\, d\bar{z} = \frac{2b^{v/2} x_T^v}{\Gamma(v)} K_v(2\sqrt{b}x_T). \tag{E.6}
$$

And the CDF may be written as,

$$
P(x) = 1 - P(x > x_T) = 1 - \frac{2b^{v/2} x^v}{\Gamma(v)} K_v(2\sqrt{b}x). \tag{E.7}
$$

The PDF and CDF for square-law detected data may be derived by substituting $z = x^2$, and carry out the same procedure. The results are given as,

$$
p(z) = \frac{2b^{\frac{v+1}{2}} z^{\frac{v-1}{2}}}{\Gamma(v)} K_{v-1}(2\sqrt{bz}), \tag{E.8}
$$

$$
P(z) = 1 - \frac{2(bz)^{v/2}}{\Gamma(v)} K_v(2\sqrt{bz}). \tag{E.9}
$$

These results are used for deriving the threshold multiplier if the clutter plus noise is assumed to be K-distributed. The theory in this appendix is taken from [3, ch.4] [28].

Appendix F

Monte Carlo Simulator

For testing of the automatic detector, a simulator was constructed using MATLAB. This is useful for making sure that the alghoritms work properly before the real radar data is applied. The basis of the simulator will be presented in this appendix. The simulator generates a noisy environment with optional distribution, and it has the ability to include single or multiple targets. The noisy environment may be interpreted as clutter with the current distribution. The targets are generated with a Gaussian antenna diagram and a Gaussian time pulse in order to simulate Swerling case 2 targets. The noise is added to the targets. The two-way Gaussian antenna diagram is generated from the function,

$$G(\theta) = \exp\left(\frac{-2.776\theta^2}{\theta_{3\text{dB}}^2}\right), \tag{F.1}$$

where θ is the current angle, and $\theta_{3\text{dB}}$ is the 3 dB beamwidth. The Gaussian time pulse generated from the function is,

$$f(t) = \exp\left(-1.386\left(\frac{t}{\tau}\right)^2\right), \tag{F.2}$$

where t is the current time instance and τ is the pulsewidth [29]. The simulated environment with two targets is shown in Figure F.1 with target SNR=10 dB for both targets.

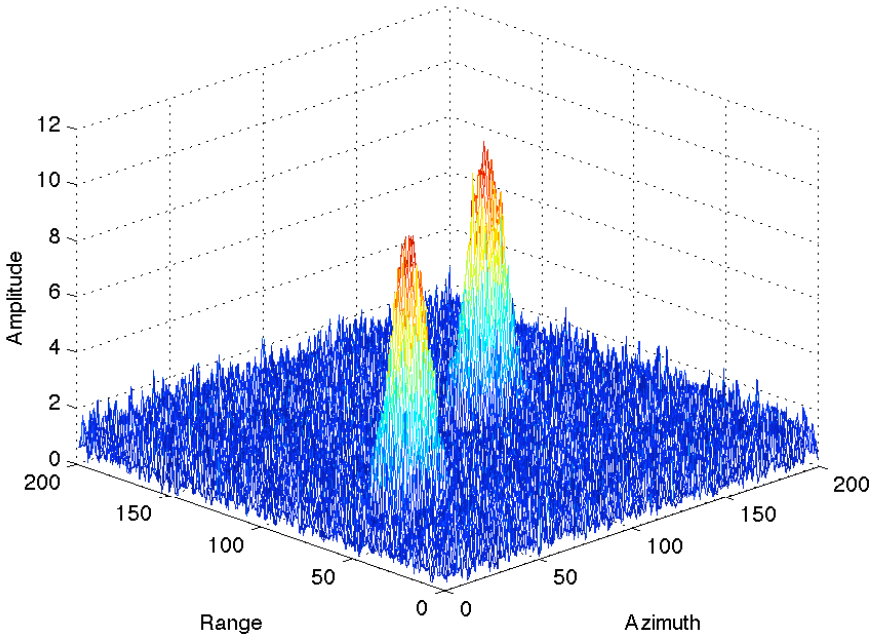

Figure F.1: Plot of simulator output with two targets in Exponential distributed noise.

Appendix G

MATLAB Code

In this appendix, the MATLAB code developed for the operation of the automatic detector is shown. Also, the code used for ML estimation and numerical integration for K-distribution are given. The numerical integration method was also applied similarly to Log-Normal distribution by changing the expressions for PDF and CDF, but it is not shown here.

G.1 OS_CFAR.m

```
function [HitM,Hitpercentage]=OS_CFAR(Data,N,k,alpha)


% The function carries out the operation of the OS CFAR. The input is MTI
% processed sample matrix, where each column represents a pulse and each
% row represents a range instance. The CFAR parameters are N, k and alpha,
% where alpha is the predetermined CFAR multiplier. The output is a binary
% matrix containing the detections, and the estimated false alarm
% probability.

% thrs_mat is a matrix storing the calculated threshold for each sample.
[m n]=size(Data);
thrs_mat=zeros(m,n);

% ---------------------------- OPERATION -----------------------------------------
% The next double for loop will generate the adaptive threshold pulsewise.
% The outer loop feeds the pulses, and the inner loop executes the
% operation for each range sample.


for j=1:n

    for i=(N/2)+1:m-(N/2)

        % Extracting reference window.
        ref_win=Data([i-(N/2):i-1 i+1:i+(N/2)],j);
        % Sorting the reference window.
```

```
28          sort_win=sort(ref_win);
29          % Selects the k'th value in the sorted window.
30          Xk=sort_win(k);
31          % Computing the threshold.
32          thrs_mat(i,j)=alpha*Xk;
33
34      end
35  end
36
37  thrs_mat=thrs_mat(N/2+1:end-N/2,:);
38  Data=Data(N/2+1:end-(N/2),:);
39
40
41  % ---------------- DETECTION OF THRESHOLD CROSSINGS -------------------------------
42
43  % Threshold crossings are detected by the function bsxfun. The function
44  % returns a binary matrix containing 1's at the position where the
45  % threshold is crossed, and 0's otherwise. The magnitude of the threshold
46  % crossings are restored in the Pow_hit matrix. Furthermore, the
47  % coordinates of the detections are retrieved by the find function.
48
49  % Returns a binary matrix which indicates threshold crossings.
50  HitM=bsxfun(@gt,Data,thrs_mat);
51
52  % Calculating the hit percentage as an estimate of false alarm probability.
53  % (This is only valid if the input contains clutter plus noise only).
54  Numberofhits=numel(HitM(HitM==1));
55  Hitpercentage=Numberofhits/numel(HitM);
56
57  end
```

G.2 Binary_integrator.m

```
1   function [BinM, successPercentage]=Binary_integrator(HitM,n,m)
2
3   % The function carries out the operation of the binary integrator. The
4   % input is a binary matrix containing detections after CFAR detection. Each
5   % column represents a pulse, and each row represents a range instance. The
6   % parameters are m and n, where m is the number of detections required to
7   % declare target presence. The output is a binary matrix containing the
8   % detections, and the successPercentage is an estimate of the false alarm
9   % probability.
10
11  [k l]=size(HitM);
12  successCount=0;
13  BinM=zeros(k,l);
14
15  % ------------------------------ OPERATION ---------------------------------------
16  % The outer for loop feeds the rows and stores the detections after
17  % integration in BinM. The inner for loop compares the current column and n
18  % consecutive columns to the threshold m for each step. If the number of
19  % 1's in the i'th column and n consecutive columns is larger than m,
20  % successCount is incremented by 1.
21
22
23  for j=1:k
24
25      % Clearing storing vector for the k'th row.
26      RangeStore=zeros(1,l);
```

```
27
28      for i=1:l-(n-1)
29
30          % The sum of the elements in the i'th column and n consecutive
31          % columns.
32          TMPsum=sum(HitM(j,i:i+(n-1)));
33
34          % Comparison with the threshold m.
35          if TMPsum>=m
36
37              % Increments the the number of successes.
38              successCount=successCount+1;
39              % Storing the detections.
40              RangeStore(i:i+(n-1))=HitM(j,i:i+(n-1));
41
42          end
43
44      end
45
46      % Storing detections in k'th row.
47      BinM(j,:)=RangeStore;
48
49  end
50
51  % ---------------------------- DETECTIONS ----------------------------------------
52  % Calculating the success percentage as an estinate of false alarm
53  % probability. (This is only valid if the input contains clutter plus noise
54  % only).
55
56  NumberofTrialSets=k*(length(HitM)-(n-1));
57  successPercentage=successCount/NumberofTrialSets;
58
59  end
```

G.3 K_ML_estimator.m

```
1   function [MLE_B MLE_V] = K_ML_estimator(Data,b,v)
2
3   % The function calculates the maximum likelihood of the scale and shape
4   % parameter for K distribution. The input is a matrix of square-law
5   % detected data, and two vectors. The vectors contains the range of scale
6   % and shape parameters that are to be applied. The output is the
7   % combination of parameters that yields the maximum likelihood.
8
9   % Converting the matrix Data to a vector.
10  z=Data(:);
11
12  % ------------------- GENERATION OF PARAMETER LIST ---------------------------
13  % The parameters in vector b and v is combined in a matrix with 2 rows and
14  % b*v columns. Thus, the resulting matrix contains all combinations of the
15  % parameters.
16
17  P1L=length(b);
18  P2L=length(v);
19
20  P1_mat=ones(1,P2L)'*b;
21  P1_mat=P1_mat(:)';
22
23  P2_mat=v'*ones(1,P1L);
```

```
P2_mat=P2_mat(:)';

P_list=zeros(2,length(P1_mat));
P_list(1,:)=P1_mat(:);
P_list(2,:)=P2_mat(:);

% ---------------------- CALCULATING LOGARITHMS ----------------------------------
% The logarithm of the PDF is calculated for each set of parameters using a
% for loop. The results is stored in a matrix TMP.

TMP=zeros(length(z),length(P_list));

for i=1:length(P_list)

    % Declaring variables.
    B=P_list(1,i);
    V=P_list(2,i);

    % Calculating the logarithm of the expression for K-distribution after
    % square-law detection for the i'th set of parameters.
    TMP(:,i)=log(((2*B^((V+1)/2).*z.^((V-1)/2))./gamma(V)).*besselk(V-1,2.*sqrt(B.*z)));

end

% ---------------------- CALCULATION OF ML ---------------------------------------
% The sum of logartihms for each set of parameters is calculated, and the
% index of the corresponding maximum likelihood is found.
lhood=sum(TMP);
max_combo=find(lhood==max(lhood(:)));

% The ML parameters are extracted from the parameter matrix.
MLE_B=P_list(1,max_combo);
MLE_V=P_list(2,max_combo);

end
```

G.4 OS_K_integrator.m

```
function [ALPHA, check] = OS_K_integrator(B,V,N,k,Pfa)

% The function carries out numerical integration for the OS CFAR expression
% for Pfa. The input is K-distributed. The inputs are the scale parameter B
% and the shape parameter V, the number of reference samples N and the
% choice of k'th value. The same method may be applied for other integrals
% as well by changing the expressions.

% ---------------- DEFINING THE EXPRESSION FOR PFA -----------------------------
% The PDF and CDF of the K-distribution for square-law detected samples are
% defined as functions of z.
p=@(z) ((2*B^((V+1)/2)*z.^((V-1)/2))./gamma(V)).*besselk(V-1,2.*sqrt(B.*z));
P=@(z) 1-(((2*(z.*B).^(V/2))./gamma(V)).*besselk(V,2.*sqrt(B.*z)));

% The PDF of the test cell including the CFAR multiplier is defined as a
% function of z and the CFAR multiplier.
Pt=@(z,alpha) 1-(((2*(sqrt(alpha.*z.*B)).^V)./gamma(V)).*besselk(V,2.*sqrt(B.*alpha.*z)));

% The binomial coefficient in the expression for Pfa for OS CFAR is
% defined.
Const=factorial(N)/(factorial(k)*factorial(N-k));
```

```
22
23 % The expression for Pfa is defined by combining the previous functions.
24 % The expression is a function of z and the CFAR multiplier.
25 f=@(z,alpha) k*Const*p(z).*P(z).^(k-1).*(1-P(z)).^(N-k).*(1-Pt(z,alpha));
26
27 % ---------- NUMERICAL INTEGRATION ----------
28 % The numerical integration of the expression for Pfa is carried out using
29 % Lobatto quadrature. The integral is evaluated on the CFAR multiplier
30 % alpha. The range of integration must be defined for each value of alpha.
31 % If not, erroneous estimates may be produced. The range may be decided by
32 % evaluating a plot for some range of z.
33
34 % Figure for evaluating the range of integration. The value of alpha must
35 % be defined in the vicinity of the true value. This is merely carried out
36 % by trial and error.
37 z=1:0.1:500;
38 figure;
39 plot(z,f(z,1));
40 grid;
41
42 % Numerical integration using Lobatto quadrature. The range must be defined
43 % for each value of alpha that is to be calculated.
44 intF=@(alpha) quadl(@(z) f(z,alpha), 30 ,300);
45
46
47 % ---------- SOLVING ALPHA FOR A GIVEN VALUE OF PFA ----------
48 % The value of alpha is located where the integrated function equals Pfa.
49 % This is found using fsolve, which finds the value where
50 % intF(alpha)-Pfa=0.
51
52 % Specification of the accuracy when using fsolve.
53 opts=optimset(optimset('fsolve'), 'TolFun', 1e-20, 'TolX', 1e-20);
54
55 % Finding the CFAR multiplier ALPHA. A value is defined as a starting point
56 % for the fsolve algorithm.
57 ALPHA=fsolve(@(alpha) (intF(alpha)-Pfa), 20,opts);
58
59 % Controlling that the correct Pfa is obtained.
60 check=intF(ALPHA)
61
62 end
```